Spring 4-14-2022

Utilizing Sensitivity and Correlation Coefficients from MCNP and Whisper to Guide Microreactor Experiment Design

Alexis Maldonado
The University of New Mexico

Alexis Maldonado
Candidate

Nuclear Engineering
Department

This thesis is approved, and it is acceptable in quality and form for publication:

Approved by the Thesis Committee:

Christopher Perfetti, Chairperson

Holly Trellue

Forrest Brown

UTILIZING SENSITIVITY AND CORRELATION COEFFICIENTS FROM MCNP AND WHISPER TO GUIDE MICROREACTOR EXPERIMENT DESIGN

by

ALEXIS MALDONADO

BACHELOR OF SCIENCE IN NUCLEAR ENGINEERING
TEXAS A&M UNIVERSITY, 2019

THESIS

Submitted in Partial Fulfillment of the
Requirements for the Degree of

Master of Science
Nuclear Engineering

The University of New Mexico
Albuquerque, New Mexico

May 2022

Dedication

First, I would like to thank my parents, Aracely y Abigael, who have always supported my academic endeavors. Es un honor ser su hijo y soy muy agradecido por todo. I would like to thank my siblings for growing up with me; I hope we will continue to learn from each other. To all my friends, thank you for enabling me to be the best version of myself; our late-night chats will always be remembered and cherished. I would also like to thank my extended family. Gracias a mis abuelos, abuelas, tios, tias, primos, y primas quienes ayudaron a criarme. Words alone are not enough to express how grateful I am to my family and friends.

Finally, I would like to thank my significant other, Francine. Your love and support will never go unnoticed. Thank you for being my partner in this journey and I am always looking forward to our next adventure.

Acknowledgements

I would like to thank my research advisor Professor Christopher Perfetti. I know I ask a million questions and I am grateful that you have the patience to respond with a million answers. Additionally, I would like to thank my professors and teachers throughout my academic career. Thank you for imparting your knowledge and lessons; I hope to continue to learn and grow.

Thank you to my work mentors Holly Trellue and Mikaela Blood from Los Alamos National Laboratory. In addition to the technical knowledge you have taught me, both of you have helped me find my role in the group. Thank you to everyone at NEN-5 and anyone who has acted as a professional mentor to me at any level. I hope to work on many more interesting projects and continue to learn from all of you.

Research presented was supported by the Laboratory Directed Research and Development program of Los Alamos National Laboratory under project numbers 20210801ER "Prediction Improvements of Transient Behavior in Advanced Reactors" and 20220084DR "Next Generation Small Nuclear Reactors." The NCERC facility is supported by the DOE Nuclear Criticality Safety Program, funded and managed by the National Nuclear Security Administration (NNSA) for the DOE. This work was supported by the US Department of Energy (DOE) through the Los Alamos National Laboratory. Los Alamos National Laboratory is operated by Triad National Security, LLC, for the National Nuclear Security Administration of U.S. Department of Energy (Contract No. 89233218CNA000001). Approved for unlimited release under LA-UR-22-23275.

UTILIZING SENSITIVITY AND CORRELATION COEFFICIENTS FROM MCNP AND WHISPER TO GUIDE MICROREACTOR EXPERIMENT DESIGN

by

Alexis Maldonado

B.S., Nuclear Engineering, Texas A&M University, 2019

M.S., Nuclear Engineering, The University of New Mexico, 2022

Abstract

When designing experiments for full-scale reactor systems, MCNP®* and Whisper can be used to create neutronic models and compare the similarity of two nuclear systems via correlation coefficients for k_{eff}, effective multiplication factor. This thesis applies this framework to a conceptual heat-pipe, yttrium-hydride moderated microreactor system and experiments. The framework is intended as a supplement to other neutronics/thermal/multiphysics analyses and provides a concrete method to measure the neutronic similarity of two systems. By analyzing the shared nuclear data uncertainty, as well as sensitivity to nuclear data over all neutron energies, highly informative experiments can be designed to aid in the development of microreactor and other advanced reactor technologies and systems.

Keywords: Microreactors, experiment design, sensitivity and correlation coefficients, neutronics, neutron transport, MCNP, Whisper

---

Table of Contents

Chapter 1 - Introduction *1*

Section 1.1. Research Objective **5**

Section 1.2. Methodology **6**

Chapter 2 –Background and Description of Snowflake Design *8*

Section 2.1. History of Microreactors **8**

Section 2.2. Heat-pipe Microreactor Snowflake **12**

Section 2.3. Heat pipes **15**

Section 2.4. Moderators **18**

Section 2.5. Fuel **22**

Section 2.6. Beryllium Oxide Reflector, Control Drums, and Shielding **25**

Chapter 3 – Physics Codes and Theory *27*

Section 3.1. MCNP **27**

Section 3.2. The Neutron Transport Equation **30**

Section 3.3. Sensitivity Coefficients and First-Order Perturbation Theory **36**

Section 3.4. Correlation Coefficients and Whisper **44**

Chapter 4 - Methodology *46*

Section 4.1. Experimental Facility **46**

Section 4.2. Proposed Microreactor Experiments **48**

Section 4.3. Proposed Analyses **55**

Chapter 5 - Results *57*

Section 5.1. Neutron flux and percentage of neutrons causing fissions analyses.....57

Section 5.2. Sensitivity coefficient analyses.....70

Chapter 6 – Conclusion ***..... 77***

References ***..... 80***

Chapter 1 - Introduction

With the increasing need for electricity while facing the challenge (and threat) of climate change, there is currently one power source that can scale up according to global need while remaining stable, safe, clean, and scalable. Nuclear energy relies on the generation of heat during nuclear fission within appropriate materials, such as uranium, to produce electricity. Most commonly, commercial nuclear reactors are light water reactors that boil water to spin steam turbines that connect to a generator. Historically, light water reactors have done their job well and are currently producing about 10% of global electricity (28% of all low-carbon power) [1], while remaining one of the safest sources of energy with regards to deaths per terawatt-hour [2].

Nuclear energy is unique in its position of being a stable, scalable power source while remaining safe and clean. Solar energy is safe, clean, and scalable but at the cost of large amounts of land and materials such as rare earths and critical metals needed for photovoltaics. Wind is also safe, clean, and scalable at the cost of large amounts of land. What solar and wind energy truly lack at the moment is stability as a power source; solar and wind are an intermittent power source that need the sun to be shining or the wind to be blowing. Until an efficient energy storage solution is implemented years from now, wind and solar energy can only serve a small percentage of our energy needs. Hydro power is stable, safe, and clean, but is not scalable; only certain locations are suitable to dam up, with the most promising locations already producing electricity. Any other power source either produces higher orders of magnitude more deaths per terawatt-hour or higher orders of magnitude more tons of greenhouse emissions. At the given moment, nuclear energy has the unique value proposition of being the only power source that is stable, safe, clean, and scalable.

Regardless, nuclear energy continues to innovate and advance. Light water reactors have a stellar track record, as mentioned in the previous paragraphs. However, light water reactors cannot meet all of the evolving needs of advanced fuel cycles. Light water reactors tend to operate below 600 Kelvin (620° Fahrenheit) and require large amounts of water. This means light water reactors cannot generate process heat that requires higher temperatures in the manufacturing industry; light water reactors will not be operating in remote areas where there is no water supply; light water reactors will not take us to Mars, the outer reaches of our solar system, or beyond. We have just scratched at the potential of nuclear energy and much work remains to be done.

Advanced reactor technologies and designs seek to meet the needs that light water reactors cannot meet. One such advanced reactor is the microreactor, a small nuclear reactor that can generate up to 20 megawatts of thermal power. Microreactors are intended to be small enough to be hauled by a semi-trailer truck, flown via plane, or shipped via boat to allow for deployment in remote regions as shown in Figure 1. Since microreactors are intended to be integral units, i.e., the microreactor will contain the fuel, heat transfer mechanism, and electricity conversion systems all encapsulated in the reactor module/modules, microreactors can serve as the sole source of heat/electricity, power a microgrid, or connect to a large-scale electric grid.

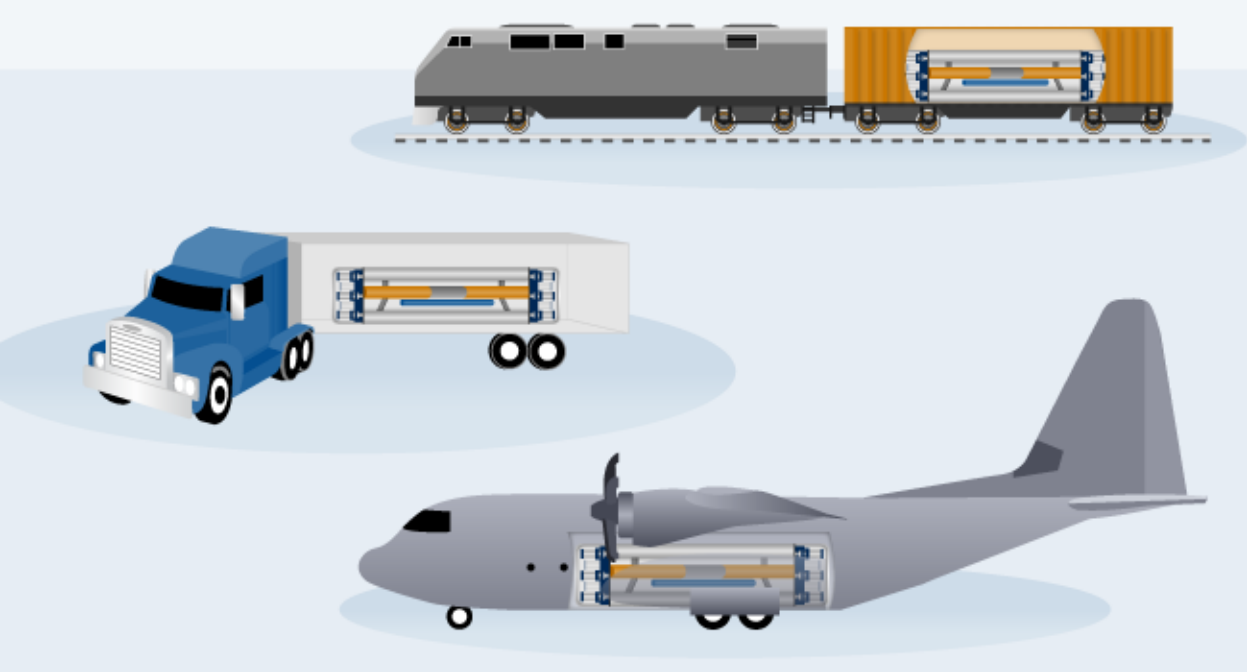

Figure 1. Microreactor shipping options [3]

Microreactors can serve many needs both on Earth and in space. Terrestrial applications for microreactors include electricity or heat generation in remote regions such as locations approaching the Arctic circle where electricity infrastructure is less developed due to harsh terrain and conditions. Microreactors, because of their smaller size, can also be designed to be mobile; such applications include power generation for oil exploration or military operations in remote regions that may move around. Rapid deployment of electricity due to the integral design can also be tremendously helpful in disaster relief; a region that is struck by a hurricane may have had their electric infrastructure destroyed. Electricity saves lives, especially after natural disasters strike; a microreactor on a ship that can be deployed after the storm passes can save many people. In space, microreactors can also play a large role. A microreactor can be designed to produce electricity for ion propulsion; nuclear electric propulsion, in conjunction with traditional space propulsion methods, can allow humans to go deeper in space due to the high

energy density of nuclear materials. A microreactor can also be designed to provide surface power on the Moon, Mars, or some other human outpost in space due to their small size, which would allow the microreactor to be stowed away on a space ship.

Regardless of the many needs microreactors can meet, novel nuclear designs will always require rigorous modeling/simulation, analysis, and experimentation in order to prove feasibility, ensure safety, and meet budgets. Nuclear experiments in particular are essential for demonstrating that a system performs as expected. These experiments range from large-scale system testing to smaller representative measurements for purposes such as code validation; accurate modeling and simulation of an experiment will increase our confidence in the predictive capabilities of the code. Furthermore, small, yet representative critical experiments of a reactor design can provide reactivity and multi-physics behavior validation opportunities at a fraction of the cost of building a full-scale prototype. Facilities such as the National Critical Experiments Research Center (NCERC) offer opportunities to perform these small-scale measurements.

Section 1.1. Research Objective

Now that the need for nuclear experiments is established, a few questions arise. How do we design an experiment for a microreactor? Intuition says to use the same materials as the full-scale microreactor design. In what quantities should the materials be used? Experiments will be built at a smaller scale than the full-scale microreactor. How do we ensure sufficient reactivity? Higher enriched fuels can provide this reactivity but will lead to different material composition compared to the full-scale microreactor. How do we ensure that both systems are neutronically similar if higher enriched fuel is used and the experiment is a much smaller size than the full-scale microreactor?

The goal of this research is to provide a framework with existing physics codes (MCNP and Whisper) to generate an objective metric for neutronic similarity when comparing a microreactor system and an experiment. The framework is intended to be general enough to also be applied to other advanced reactor concepts.

Section 1.2. Methodology

MCNP is a 3D Monte Carlo particle transport code that is used in this research to calculate effective multiplication factors, neutron flux, sensitivity coefficients, and more. MCNP has had decades of development, and results have been validated with a variety of nuclear experiments [3]. Whisper is statistical analysis code that can take MCNP sensitivity coefficients and nuclear covariance data to generate correlation coefficients between a desired system and existing benchmarks from nuclear experiments. By entering the full-scale microreactor system as a benchmark in Whisper, experiment designs can be input into MCNP and Whisper to generate a correlation coefficient for the effective multiplication factor of the systems [4]. Correlation coefficients convolve both nuclear data uncertainty and the systems' sensitivity coefficients, i.e., how sensitive a system is to a perturbation to a nuclear data parameter with regards to the effective multiplication factor. Because correlation coefficients statistically analyze both systems' sensitivity coefficients and nuclear data uncertainties for every neutron-nucleus interaction available at all relevant neutron energies, correlation coefficients are a robust, objective method to measure the neutronic similarity of two nuclear systems.

While this neutronic framework can analyze any two nuclear systems with correlation coefficients, this research will focus on the design of critical experiments in support of microreactors that are cooled with heat pipe technology. "Snowflake" is one such conceptual heat-pipe microreactor design being studied at Los Alamos National Laboratory [5]. As the primary heat transfer mechanism, heat pipes are passive, reliable, and fully contain the working fluid. This research will design several experiments that could demonstrate Snowflake-type systems; their neutronic similarity via the correlation coefficient will be calculated with the neutronic framework established with MCNP and Whisper. In addition to generating a

correlation coefficient, other metrics, such as the normalized flux per unit lethargy, the sensitivity coefficients plotted with respect to neutron energy, the percentage of neutrons causing fission, and more will be studied in greater detail to investigate any patterns that may arise.

The experiments will contain a Snowflake microreactor unit cell in the center of the experiment surrounded by high-enriched uranium fuel. The use of the unit cell provides a representative sample of the full-scale microreactor while reducing the amount of fuel that needs to be fabricated. However, there is insufficient reactivity with just a single unit cell for the experiment to go critical; hence the high-enriched uranium fuel will act as a driver fuel and provide sufficient reactivity. The high-enriched uranium nitride fuel was identified as leftover fuel from SP-100 program that could reduce the fuel fabrication cost and burden for the experiment. The logistics and for obtaining the high-enriched uranium fuel, however, needs to be further explored and other options for driving criticality will be examined in the future as well.

Chapter 2 – Background and Description of Snowflake Design

Section 2.1. History of Microreactors

Microreactors, if considering the "up to 20 megawatts of thermal power" definition, can be said to have their roots in the United States Navy's nuclear submarine program (1950s), with the first nuclear submarine producing about 10 megawatts of power [6]. Microreactors are also intended to be compact enough to be hauled by a semi-trailer truck, flown by plane, or shipped by boat to allow for deployment in remote regions as shown in Figure 2.1.

Figure 2.1. Conceptual microreactor hauled by semi-trailer truck [7]

Due to these constraints, space reactor development can also be seen as a significant contributor to future designs of present day microreactor systems. One such space reactor is the Systems for Nuclear Auxiliary Power (SNAP-10A), a compact nuclear reactor that output about 30 kilowatts of power and weighed less than 300 kilograms [8]. SNAP-10A was launched into space in 1965 by the National Aeronautics and Space Administration (NASA) in conjunction with several other organizations. The development of the capillary heat pipe at Los Alamos National Laboratory in 1963 was intended for use in space reactor systems since capillary heat pipes are not adversely affected by zero-gravity environments [9].

More recent experiments have further increased the feasibility of heat-pipe microreactor systems. The Demonstration Using Flattop Fissions (DUFF) experiment was conducted by Los Alamos National Laboratory at the National Criticality Experiments Research Center in 2012. The DUFF experiment was the first Stirling engine (heat engine that operates with the cyclic compression of gases) powered by fission energy via heat pipe [10]. In 2017, the Kilowatt Reactor Using Stirling TechnologY (KRUSTY) experiment was also conducted by Los Alamos National Laboratory. KRUSTY was a prototype fission reactor that utilized heat pipes to transfer heat to a Stirling engine and output about 5-kilowatt thermal power. KRUSTY employed high-enriched uranium molybdenum fuel with a beryllium oxide reflector as shown in Figure 2.2 [11]. KRUSTY was a prototype for a space reactor intended to provide surface power for a variety of missions, such as a Moon or Mars base. Figure 2.2 shows the vacuum tube being lowered over the experiment to simulate a space environment.

Figure 2.2. KRUSTY experiment with vacuum chamber [12]

Next, the Hypatia experiment that took place at the National Criticality Experiments Research Center in 2021 measured temperature reactivity coefficients for the high-temperature candidate moderator material yttrium hydride in two different configurations and compared the experimental results with predicted MCNP results [13]. The Hypatia experiments consist of several stacks of yttrium hydride, high-enriched uranium, graphite, spacers, and heaters as shown in Figure 2.3. The purpose of a moderating material, for example a metal hydride, in a microreactor is to help thermalize neutrons and decrease the required resulting fuel mass required to achieve criticality. In particular, results from the Hypatia experiment helped increase

the technology readiness level of yttrium hydride such that it could be used more easily in microreactor designs/systems such as the heat-pipe microreactor Snowflake design.

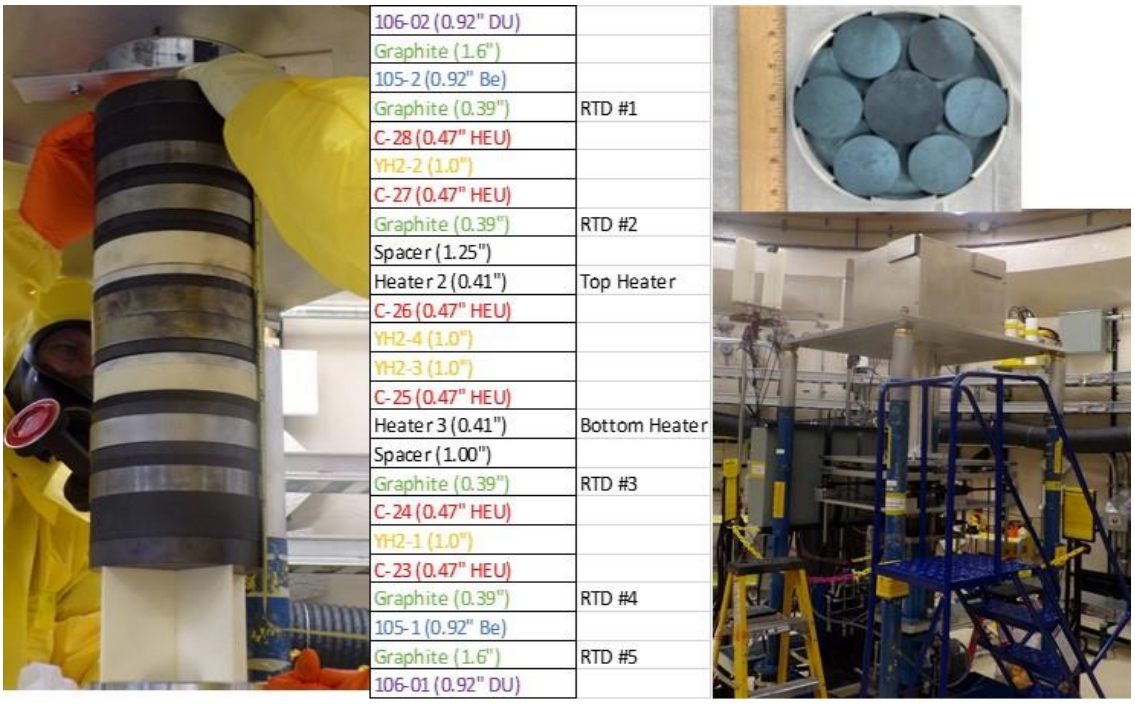

Figure 2.3. Hypatia configuration, yttrium hydride experiment [14]

While much work has been and is currently being performed to support microreactor development, additional work remains to be done to manifest these microreactor designs into reality.

Section 2.2. Heat-pipe Microreactor Snowflake

The Snowflake conceptual design comprises multiple units of 19.9% enriched uranium TRISO fuel, moderating material, and heat pipes combined in a modular fashion; the design is flexible enough to meet mission needs and can be scaled up or down depending on the power, size, or weight needed. The reactor has a higher share of epithermal neutrons causing fission than traditional light water reactors because it consists of hydride moderating material. Understanding how these epithermal neutrons interact with the reactor materials is essential for feasibility and safety of the design. As a result, there is a need to design a representative nuclear experiment for the Snowflake microreactor concept. The term unit cell in this paper is referred to as a combination of 12 fuel cylinders, 9 heat pipes (7 whole heat pipes and 6 one-third heatpipes), and 3 ovals of moderating material (6 half ovals) as shown in Figure 2.4 for the Snowflake conceptual design. These unit cells can be put together to form a full-scale reactor of different sizes to meet mission-specific needs as seen in Figure 2.5. Individual materials are described in more detail in Section 2. Instead of using partial components for the microreactor experiments, as would be the case if using only a single Snowflake design unit cell, the whole component is included as shown in the dashed line in Figure 2.4 below. This means the experiments will include 12 fuel cylinders, 13 heat pipes, and 6 ovals of moderating material.

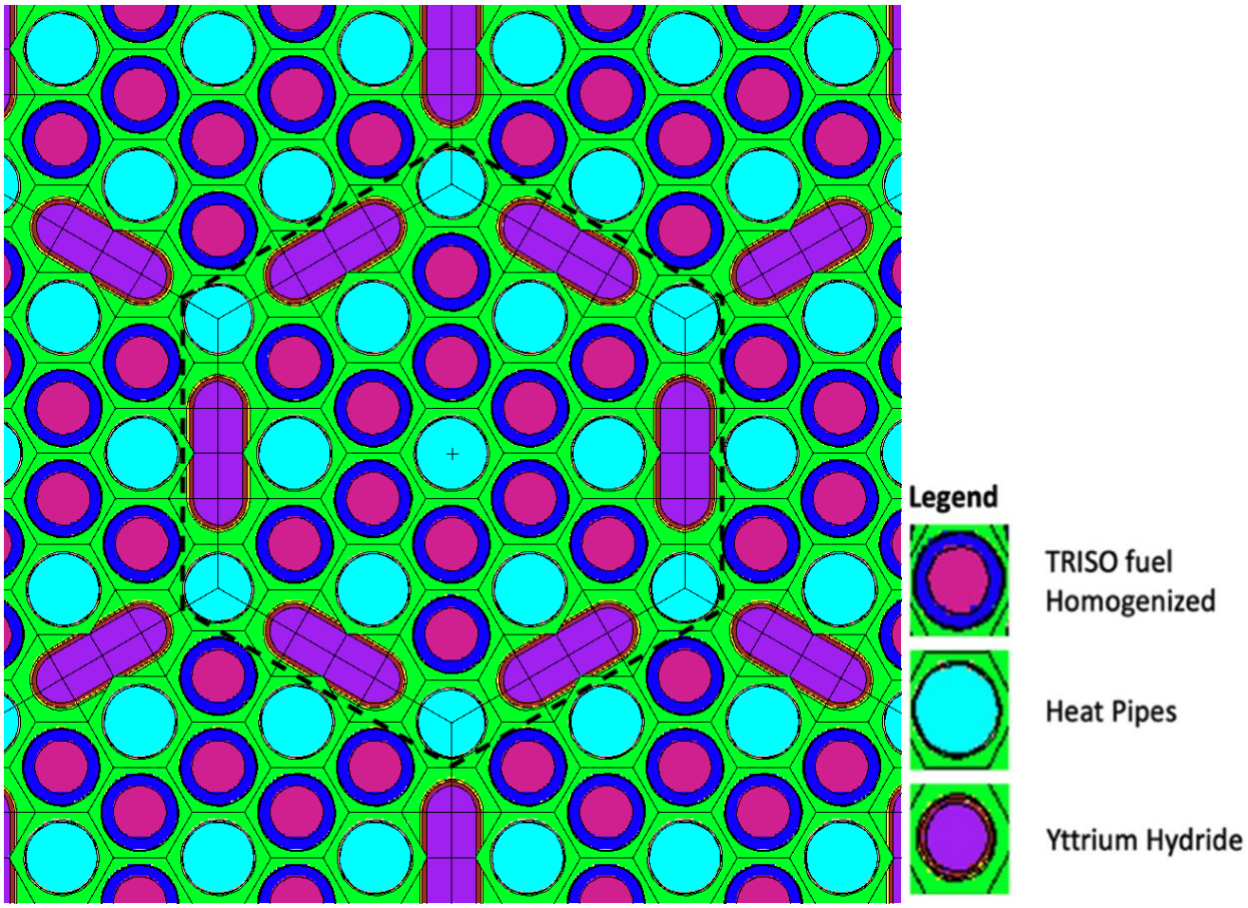

Figure 2.4. Snowflake unit cell

The full-scale microreactor Snowflake concept can also be fitted with shutdown regions near the center of the core that can allow shutdown rods filled with boron carbide to enter in case of emergency or while the microreactor is in transport.

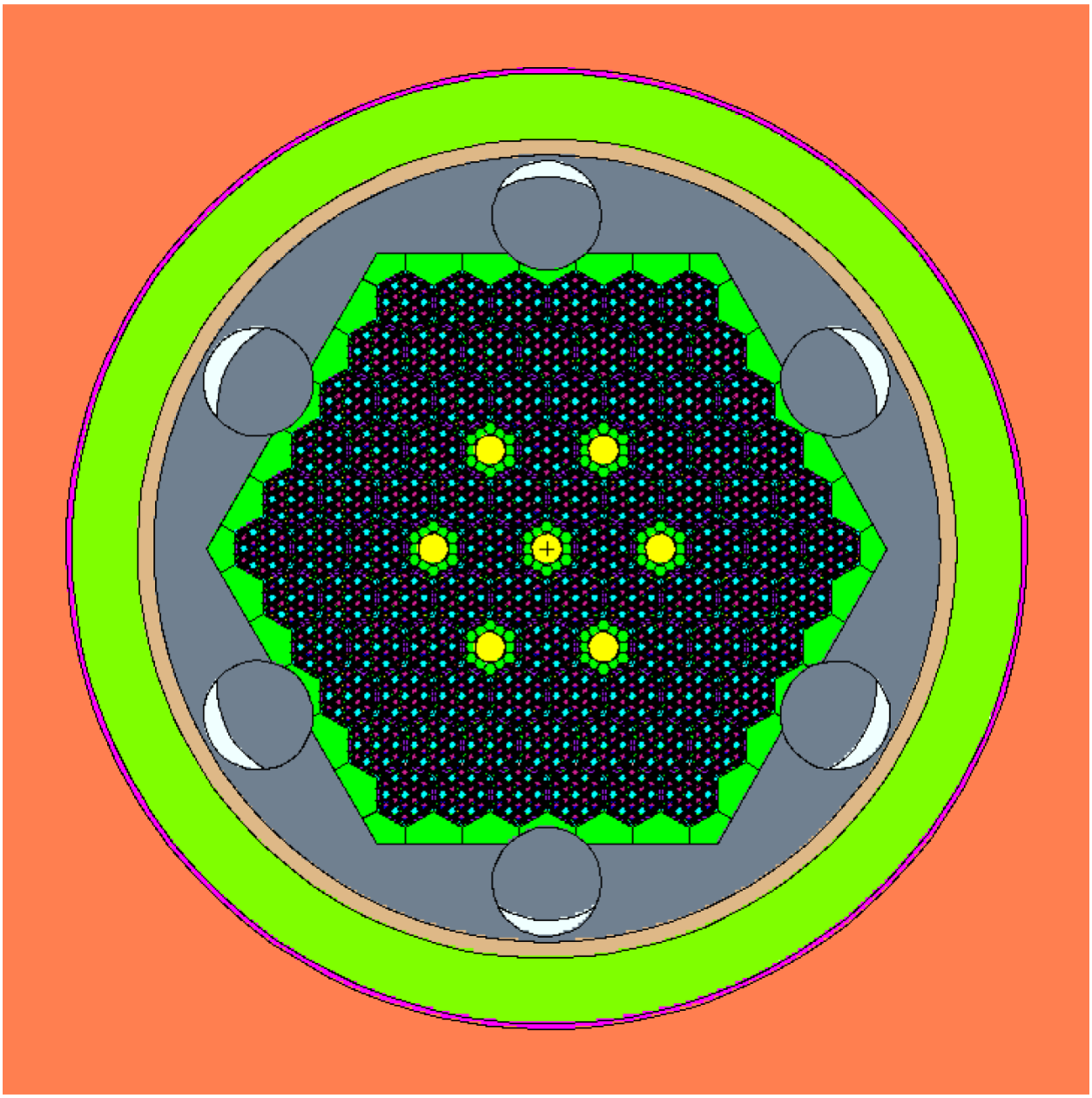

Figure 2.5. Conceptual full-scale Snowflake microreactor with control drums and shielding

Section 2.3. Heat pipes

Heat-pipe microreactors rely on heat pipes as the primary heat transfer mechanism from the core to the heat sink. Heat pipes are self-contained rods with condenser and evaporator regions that take advantage of the large amounts of energy needed to conduct a fluid phase transition to gas. A schematic of a heat pipe can be seen in Figure 2.6 below.

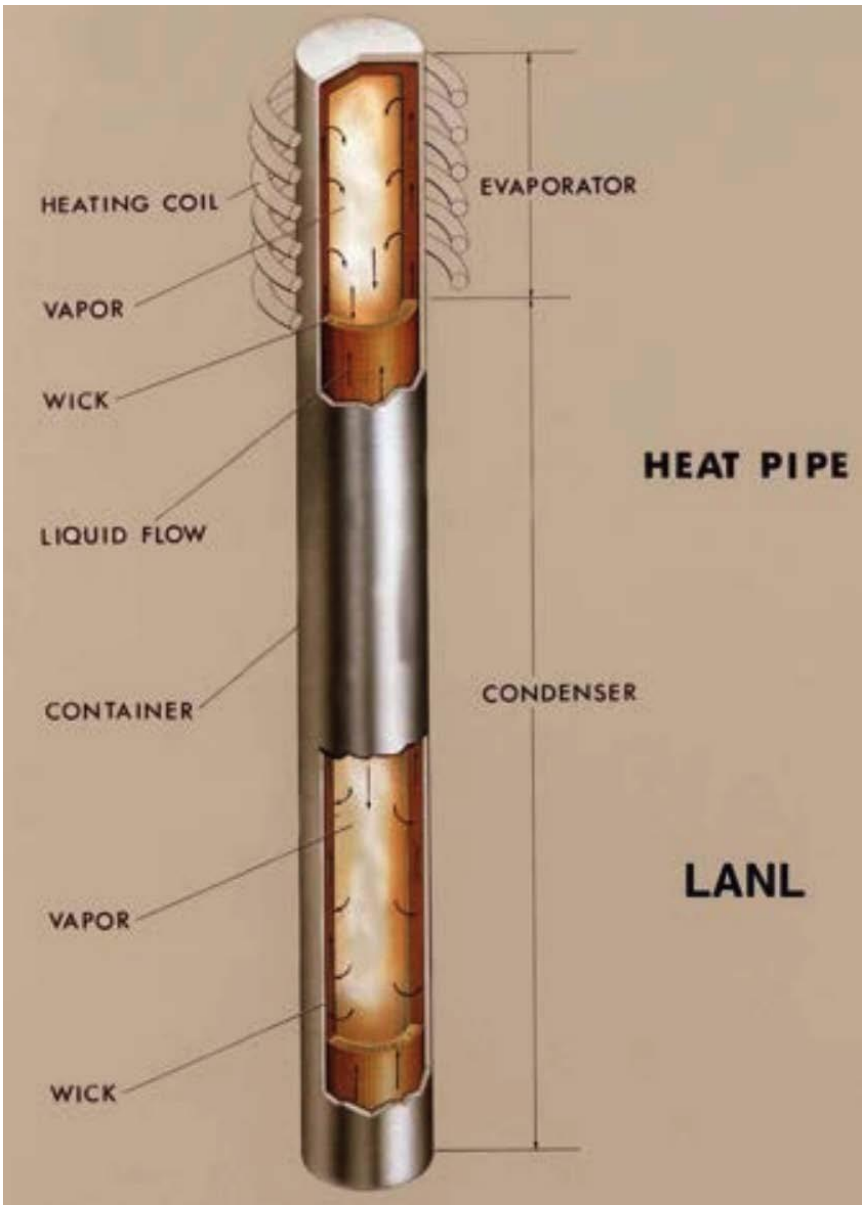

Figure 2.6. Capillary heat pipe design [15]

The first capillary heat pipes were developed at Los Alamos National Laboratory during the 1960s with the intention of using them in space reactors. Capillary heat pipes utilize a wick to separate the two-phase fluids (liquid and gas). Heat pipe microreactors can be designed to operate at higher temperatures (500°C to 1800°C) than traditional light water reactors since heat pipes can handle high temperatures as long as the appropriate working fluid inside the heat pipe is chosen. The Snowflake design uses sodium heat pipes as the primary heat transfer mechanism.

Limitations of heat pipes include the operating region shown in Figure 2.7 below. As long as the design allows for sufficient safety margin to remain within the operating region, heat pipes are highly reliable. Heat pipes are also a passive device, relying on the physics of phase transition, thermal conduction, and flow to operate. A heat-pipe microreactor can contain hundreds of heat pipes. To ensure sufficient safety margin, three adjacent heat pipes in the most vulnerable region of the reactor (i.e., the hottest region) are simulated to fail (will no longer draw heat from the core); if the remaining operating heat pipes can continue to output sufficient heat without failing, then sufficient safety margin is built into the system.

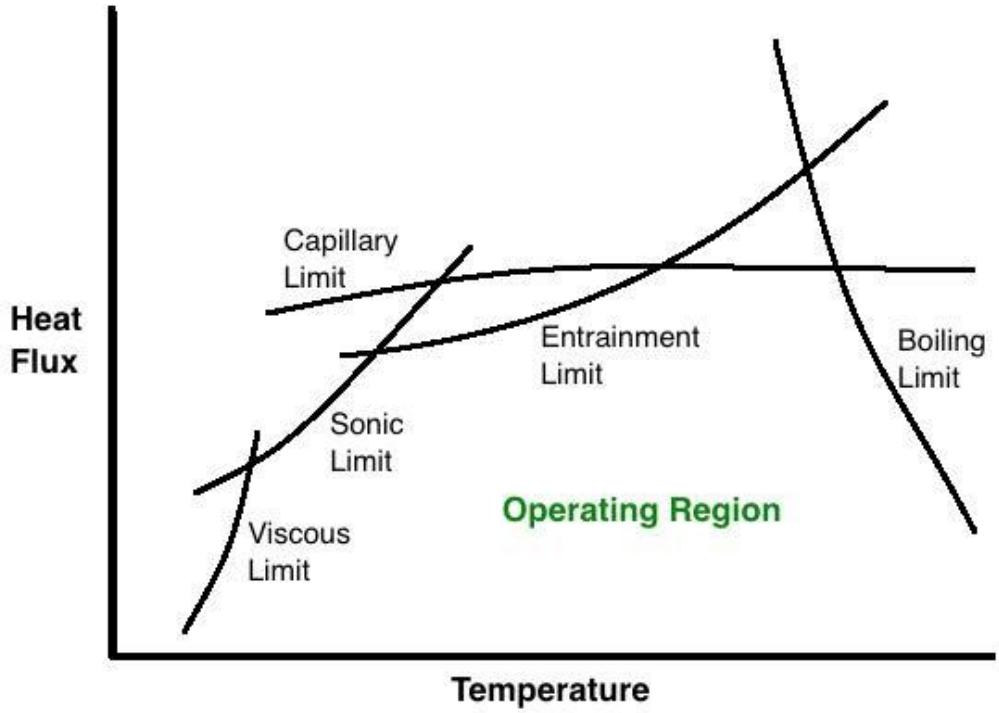

Figure 2.7. Operating region for a heatpipe [15]

Gas cooling provides an alternative heat transfer mechanism commonly proposed for microreactors. Gas-cooled microreactors take a cooled gas, such as helium, and flow the gas through channels with a pump. Potential challenges associated with gas cooling include, but are not limited to, gas leaks and pump failures which both lead to a loss in cooling ability of the system. While gas-cooled systems have exemplary cooling capabilities and favorable neutronic properties, heat pipes are chosen as the preferable heat transfer mechanism for the Snowflake microreactor design due to their passive cooling abilities and reliability over time. These heat pipe properties are best suited for microreactor systems that plan on being in remote regions where repairs will be more difficult to conduct.

Section 2.4. Moderators

For neutron moderation, the Snowflake design utilizes yttrium-hydride. Yttrium-hydride is a metal hydride that is a promising moderator candidate for microreactors due to its high hydrogen retention at temperatures up to 1000°C as seen in Figure 2.8 below [17]. The use of yttrium hydride allows for reactor operation at higher temperatures, which allows for additional thermodynamic efficiencies when converting thermal energy into electrical energy. Furthermore, the use of a moderator allows for microreactors to retain their small size while only using high-assay, low-enriched uranium fuels instead of high-enriched uranium by slowing neutrons down and increasing the probability of fission.

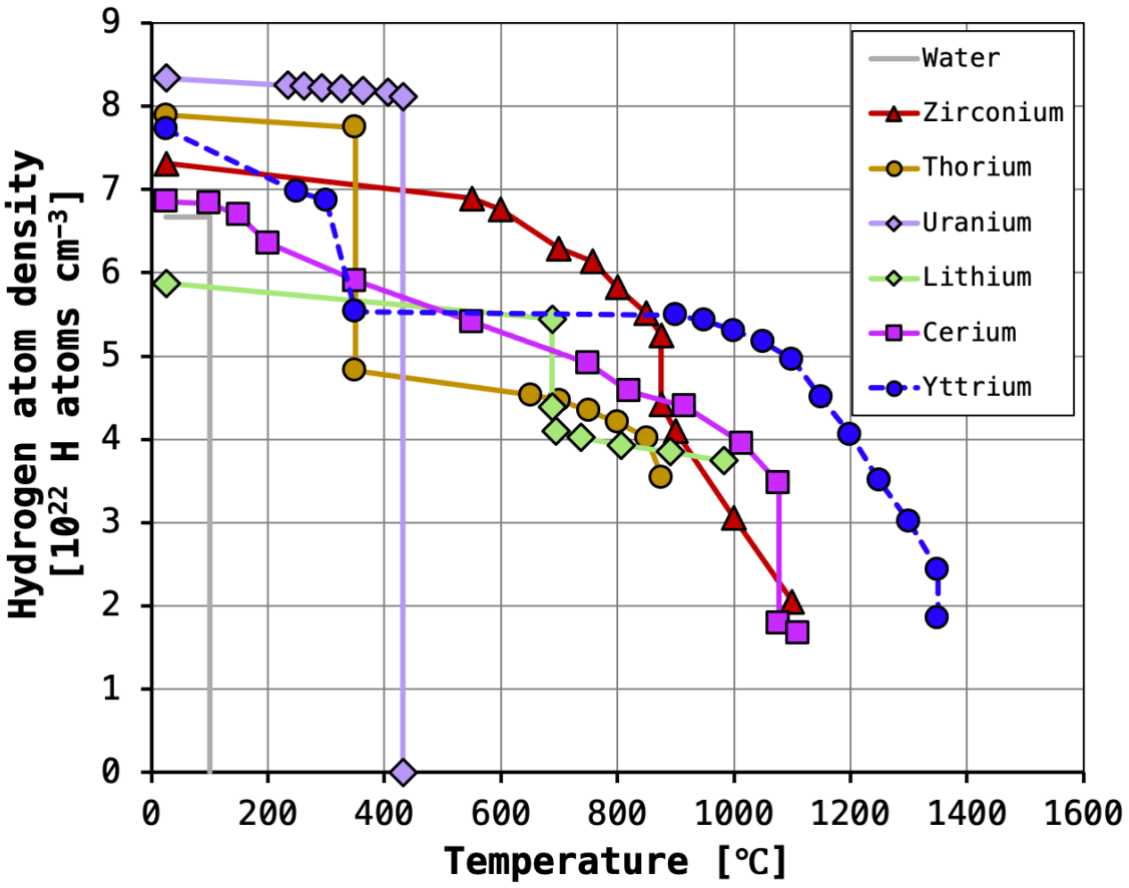

Figure 2.8. Hydrogen density with increasing temperatures of various materials [17]

A limitation to yttrium hydride is its positive temperature reactivity coefficient by itself in uranium systems due to changes in the neutron energy spectrum and competing effects of the cross sections present [17]. As yttrium hydride increases in temperature, its temperature reactivity coefficient remains positive, which means increasing the temperature of yttrium hydride will increase its reactivity worth [18]. This positive temperature reactivity coefficient (TRC) limitation of yttrium hydride is crucial to take into consideration since the overall reactor needs to have a negative temperature reactivity coefficient in order to implement negative feedback; as temperature increases, reactivity should decrease. The alternative is positive feedback (i.e., increasing reactivity with increasing temperature) which is a safety problem because increasing reactivity will increase temperature due to additional fission heating that will continue until the system overheats. Therefore, the fuel and other reactor materials must have sufficient negative temperature reactivity coefficients to cancel out the yttrium hydride effects. Further research must be conducted to assess if yttrium hydride would create localized regions that have a positive TRC and what effect, if any, this would have on the stability and controllability of the reactor system.

The primary moderating component of the yttrium hydride is the hydrogen. Since a hydrogen nucleus (a proton) is nearly the same size/mass as a neutron, a single neutron scatter off of the hydrogen nucleus may thermalize the neutron significantly as a result of fundamental kinematics and momentum transfer [13]. When studying the hydrogen cross section as seen in Figure 2.9, the hydrogen elastic scattering cross section follows the total cross section fairly closely, i.e., the neutron mostly interacts with hydrogen via scatter. Also plotted are the yttrium cross sections which are lower than the hydrogen cross sections except for some capture cross section resonances in the epithermal neutron energy ranges and some (n, 2n) and inelastic

scattering interactions at fast neutron energies. All cross sections are plotted with uncertainty, if the data is available.

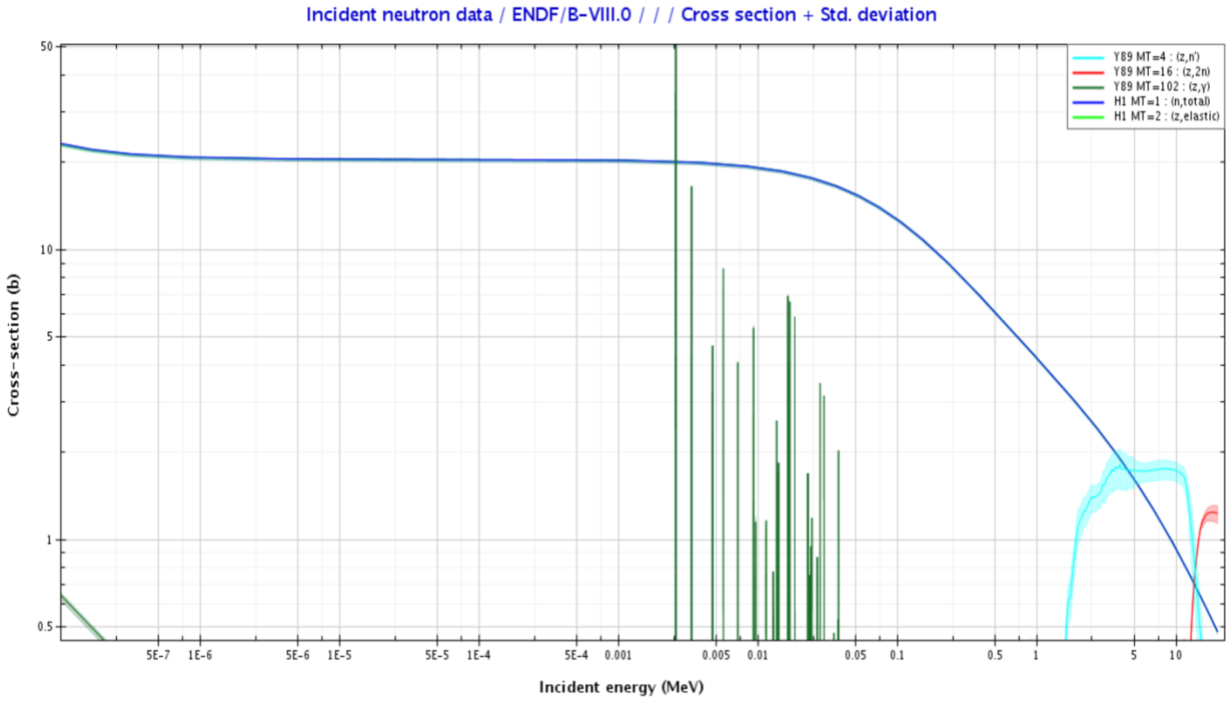

Figure 2.9. Hydrogen and yttrium cross sections [18]

Snowflake also employs a graphite monolith for both structure and neutron moderation ability. Graphite has a high melting temperature of 3600°C, making it a suitable material for high-temperature microreactors. Graphite is also a well understood reactor material than can be manufactured at large scales and cheap costs. Figure 2.10 plots the primary graphite cross sections; the most dominant cross section is the elastic neutron scattering cross section at lower neutron energies up to a little over 100 [MeV] neutron energies, which are quite rare. The parasitic absorption (gamma capture) cross section is so low, it does not appear with the given

cross section scale. The low parasitic absorption cross section and the high elastic scattering cross section makes graphite a good moderating material.

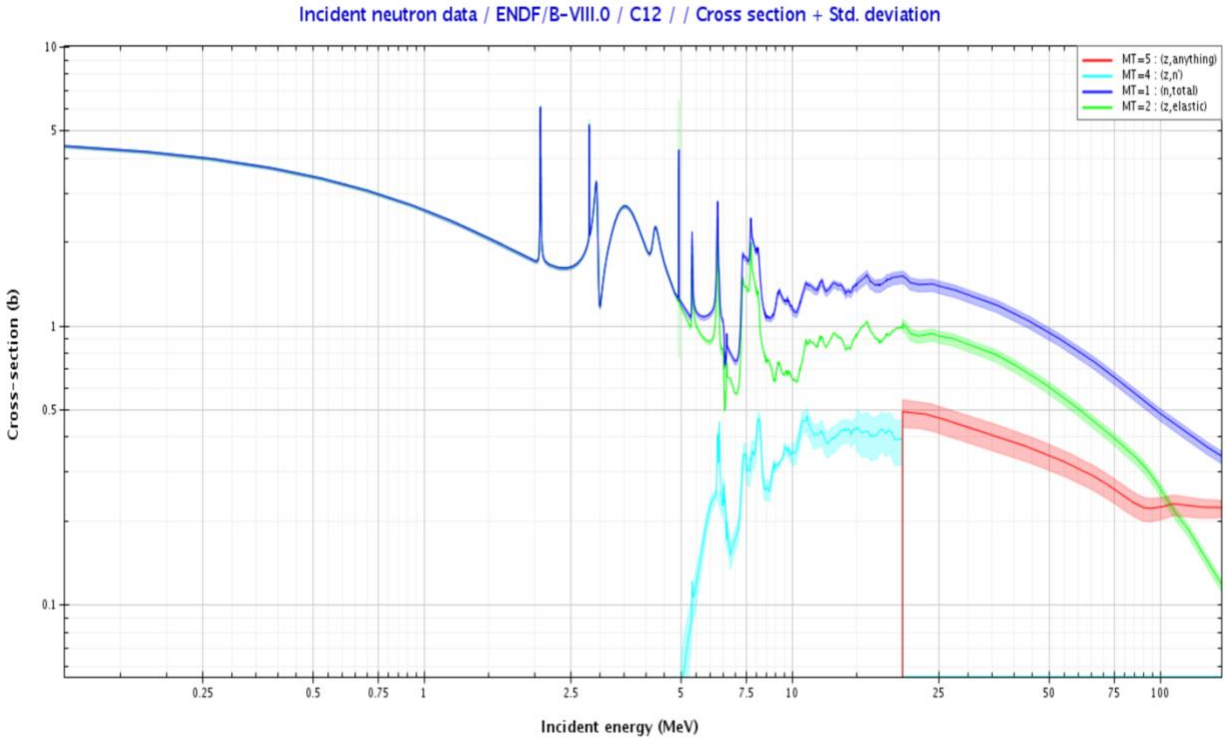

Figure 2.10. Graphite cross sections [18]

Section 2.5. Fuel

Snowflake can employ any fuel type to meet the design need; for this research, Snowflake is fitted with High-Assay, Low-Enriched Uranium (HALEU) Oxycarbide (UCO) TRi-structural ISOtropic (TRISO) fuel. HALEU fuel is low-enriched uranium which, by regulation, must contain less than 20% uranium-235 in the uranium by mass percentage. Additionally, HALEU is high-assay, which means that HALEU is typically enriched between 19.0%-19.9% uranium-235 mass percentage, a fraction that is much higher than traditional low-enriched uranium used in light water reactors (typically between 3%-5% uranium-235). HALEU fuel is typically proposed for microreactors in order to achieve a longer reactor lifetime without the need to refuel. Furthermore, HALEU fuel has a lower proliferation risk compared to highly-enriched fuel. The fuel used for this particular Snowflake design is also TRISO fuel. TRISO fuel is composed of several TRISO kernels that are tiny; about the size of a poppy seed [20]. These TRISO kernels are compacted together with graphite to form a cylindrical fuel pellet.

One computational challenge is modeling these TRISO kernels explicitly in MCNP. Since MCNP utilizes surface tracking for neutron transport, there is a significant computation slowdown when tracking neutrons in TRISO regions. One way to reduce the computational burden is to homogenize the TRISO fuel via the Reactivity equivalent Physical Transformation (RPT) method. The RPT method creates an inner, homogenized TRISO fuel region surrounded by a graphite ring as shown in Figure 2.11. The dimensions of the two regions are varied to match reactivity while keeping masses constant; many studies have been conducted to show that reaction rates and depletion with the RPT homogenization method match the explicit modeling of TRISO kernels [21]. Another method to speed up the simulation would be to employ delta tracking in MCNP; at the writing of this thesis, however, delta tracking has not been developed

for MCNP as of the latest release of MCNP6.2. As a result, the RPT method is employed to allow for rapid modeling and simulation.

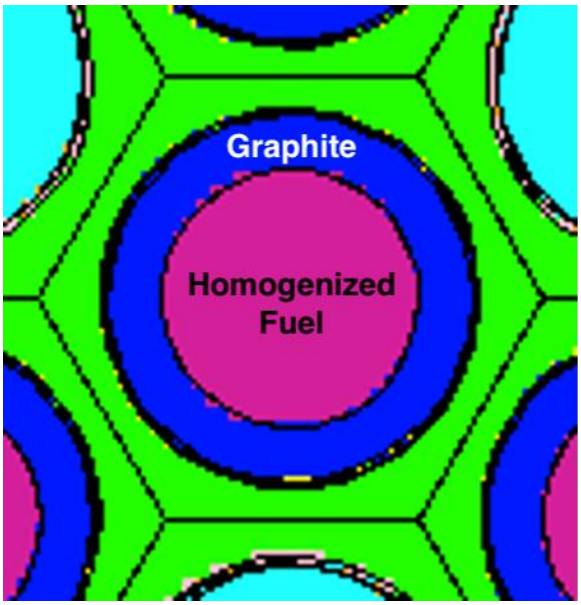

Figure 2.11. TRISO fuel homogenized via RPT method

The primary fissile nuclide of interest here is uranium-235; Figures 2.12 and 2.13 plot the uranium-235 cross sections with at different neutron energies. In moderated systems, the goal is to thermalize the neutrons as much as possible in order to take advantage of the higher fission cross section at lower neutron energy levels. The most significant competing cross section in the uranium-235 is the parasitic absorption (gamma capture) cross section. This cross section is lower than the fission cross section except for the occasional resonance in the epithermal neutron energies.

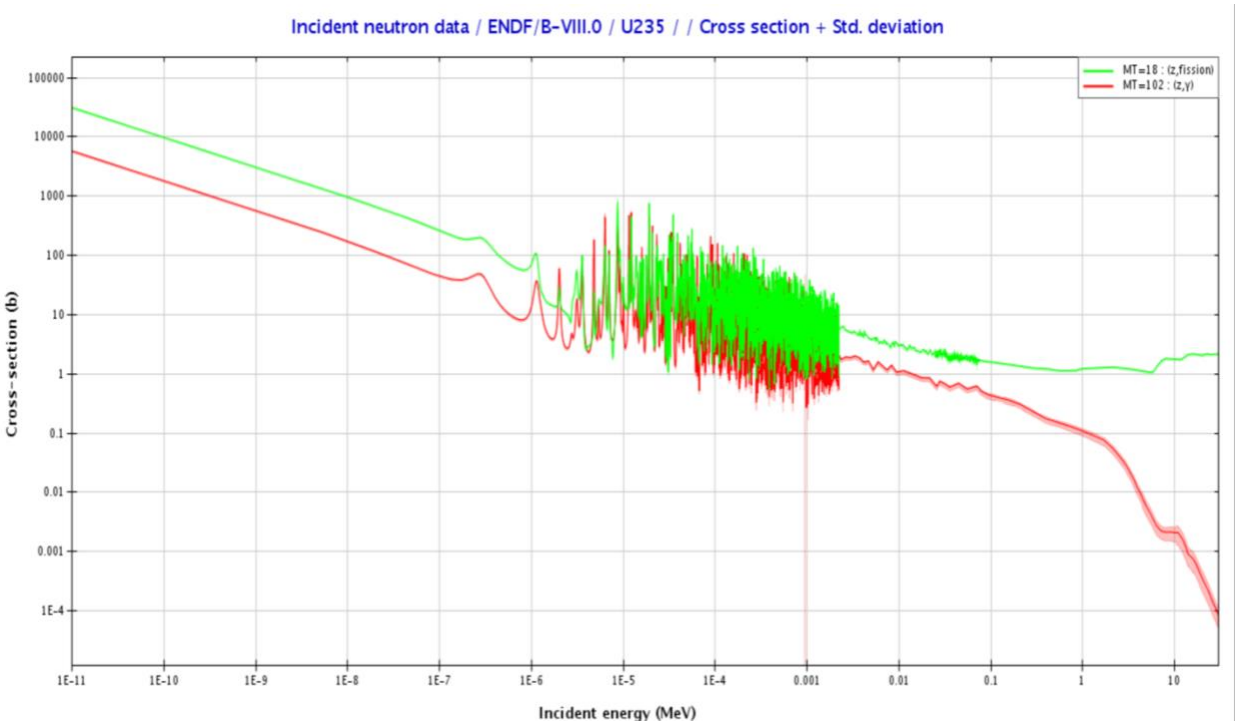

Figure 2.12. Uranium-235 cross sections, most neutron energies [18]

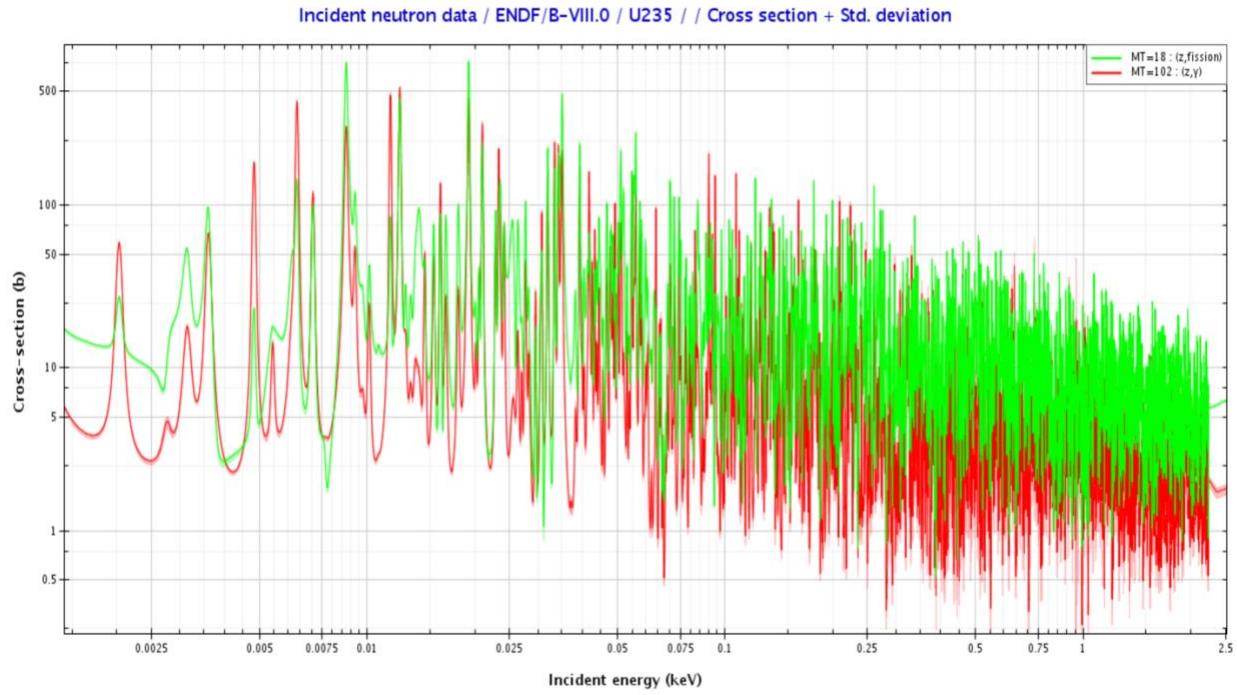

Figure 2.13. Uranium-235 cross sections, epithermal neutron energies [18]

Section 2.6. Beryllium Oxide Reflector, Control Drums, and Shielding

Beryllium oxide (BeO) is ceramic compound with attractive neutronic and thermal properties. The beryllium in the compound can act as a neutron moderator or reflector; the elastic scatter and the (n, 2n) nuclear reaction, where a neutron absorbed will release two neutrons, both play a significant role in the neutronics of the system. The cross sections for beryllium-9 are plotted in Figure 2.9 below.

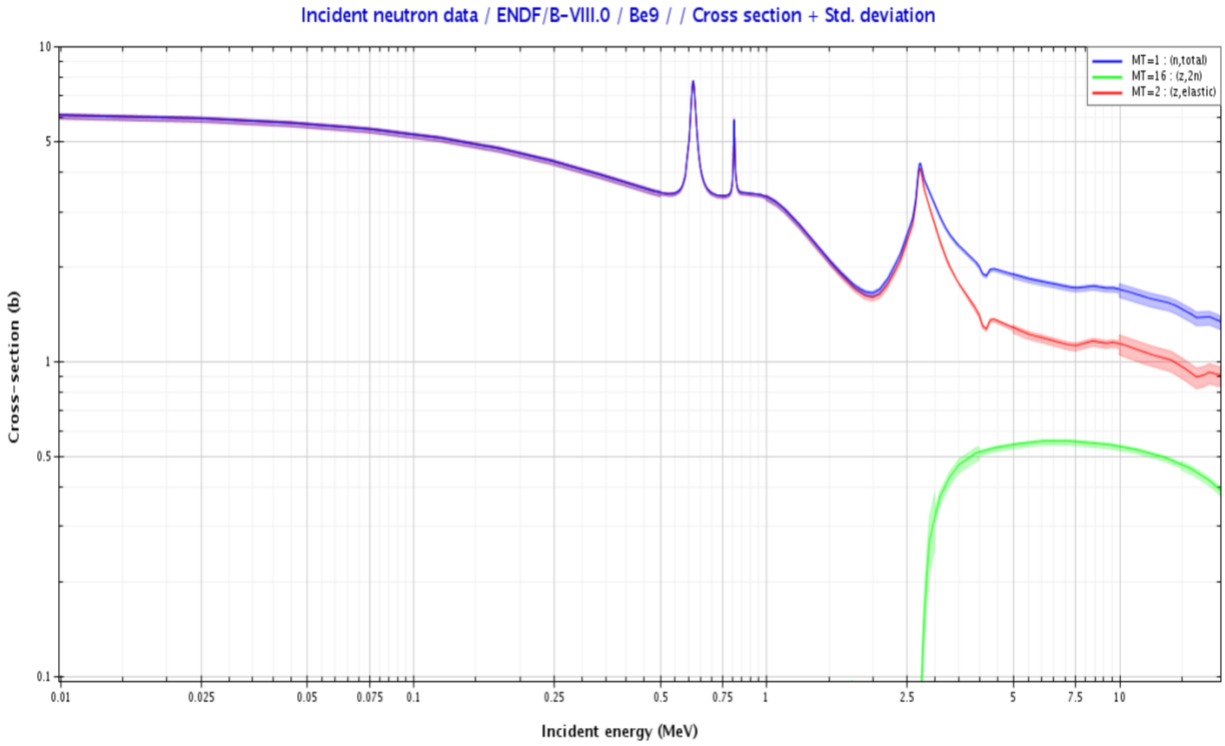

Figure 2.14. Beryllium-9 cross sections [18]

Additionally, beryllium oxide has a high thermal conductivity relative to non-metals, only beaten by diamond [21]. For the Snowflake design, beryllium oxide acts as a neutron reflector, both radially and axially.

Traditionally, light water reactors utilize control rods that are inserted into the core axially from the top or bottom and contain boron carbide (B_4C). Microreactors designs tend to utilize control drums which are placed along the circumference of the core and rotate boron carbide slices for reactivity control. The Snowflake design utilizes control drums for reactivity control as shown in Figure 2.5. The portion of the control drums that do not contain boron carbide have beryllium oxide. Control drums are rotated with engines; when the boron carbide slices are pointed outward in the maximum reactivity position, the slices also act as a neutron shield. Some microreactor designs may include regions for shutdown rods that contain boron carbide and may be inserted in case of needed negative reactivity in accident scenarios. A common accident scenario is a fully flooded reactor; to pass safety checks, the fully flooded reactor must be sufficiently subcritical when all of the shutdown mechanism are in place.

Microreactor designs typically have to consider the environment they will be operating in with regards to shielding. For space applications, weight plays an important role in determining shield materials. For terrestrial applications, cost may play a larger role for shield materials. For the Snowflake design, shielding material is flexible depending on the mission need. For this design, boron carbide is used as a neutron shield and tungsten is used as a gamma shield.

Chapter 3 – Physics Codes and Theory

Section 3.1. MCNP

MCNP (Monte Carlo N Particle) code is a stochastic radiation-transport code developed and maintained by Los Alamos National Laboratory. The Monte Carlo method simulates particles (neutrons, for this application) in a geometry specified by the user. The neutrons have a velocity and travel surface to surface during which a collision with the materials' nuclei may occur. The probability of a collision will depend on the nuclei cross section, a property that represents the cross-sectional area of the nucleus. Each possible reaction between the neutron and the nucleus can be represented as a cross section, with the sum of all possible cross sections represented as the total cross section (σ_t) of the nucleus. The Monte Carlo method takes multiple neutrons in a geometry and randomly selects numbers; the chosen numbers determine if a collision occurs which is similar to the randomness found in a casino in Monte Carlo, Monaco. Some common cross sections include the scatter (σ_s), fission (σ_f), and capture (σ_γ) cross sections. Neutrons can also "leak," i.e., escape from the geometry.

Cross sections are strongly dependent on the energy of the incident neutron. The cross sections for significant materials that will affect the system's neutronics are present in Chapter 2. Note that the cross section is reported in units of [b] or [barns] which is equivalent to 1E-24 [cm^2]; barns are useful for small nuclei cross sectional areas. Neutron energy is reported in units of [MeV] or 10^6 [eV]; electron volts is the measure of the kinetic energy gained when acceleration one electron through a 1 [V] or [Volt] potential. Electron volts are useful units of energy for particles and is equivalent to about 1.6022E−19 [J] or [Joules]. MCNP samples cross sections from nuclear data libraries, such as the Evaluated Nuclear Data File (ENDF) by the National Nuclear Data Center.

Cross sections are also material temperature dependent; commonly, cross sections experience Doppler broadening as temperatures increase. An example of Doppler broadening can be seen in Figure 3.1 where the cross-section resonance is flattened with increasing temperature. In MCNP, the effects of temperature on cross sections are factored in by specifying material temperatures in the input deck.

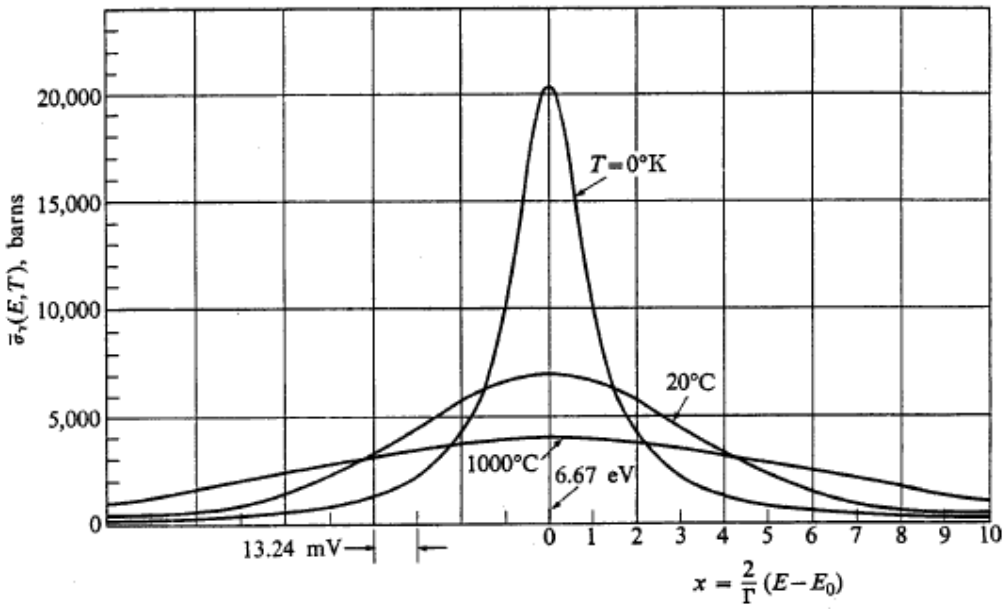

Figure 3.1. Doppler broadening of a cross section with increasing temperature [22]

As neutrons interact with the specified geometry and materials, several histories are taken and averaged to generate the most likely answer based on statistics. The central limit theorem in statistics states that in many situations with a variety of independent random variables will tend toward a normal distribution even if the independent variables themselves are not normally distributed. This means that every output from MCNP is the average result of the several hundreds of simulations and typically come with a standard deviation to denote the spread of the result. One commonly generated result is the effective multiplication factor (k_{eff}). Conceptually,

the effective multiplication factor is the ratio of the current fission neutron population to the previous generation of fission neutron population. So, a k_{eff} = 1 would be a critical system, where the fission neutrons are stable and able to replace themselves with each generation over time. A k_{eff} > 1 represent a supercritical system where the neutron population continues growing with each generation by that factor and a k_{eff} < 1 is a subcritical system where the neutron population decreases each generation by that factor. MCNP computes three k_{eff} values via different methods: the collision estimate, the absorption estimate, and the track length estimate. MCNP computes the final k_{eff} based on the combined k_{eff} values [3]. The steady-state, i.e., time-independent k_{eff} value is computed in MCNP with the KCODE input line.

Section 3.2. The Neutron Transport Equation

The neutron transport equation describes the motion and interaction of neutrons in a system, such as a nuclear reactor. The equation is a form of the Boltzmann transport equation that uses the probability distribution of various neutron-nuclei interactions and neutron behaviors to describe the system. The time-dependent neutron transport equation can be seen as a balance equation, where the gains and losses of neutrons are accounted for with each term as seen in equation (1) below [23].

$$\left(\frac{1}{v(E)}\frac{\partial}{\partial t} + \hat{\Omega}\cdot\nabla + \Sigma_t(r,E,t)\right)\psi(r,E,\hat{\Omega},t)$$
$$= \frac{\chi_p(E)}{4\pi}\int_{4\pi} d\Omega' \int_0^{\infty} dE'\ v_p(E')\,\Sigma_f(r,E',t)\,\psi(r,E',\hat{\Omega}',t)$$
$$+ \sum_{i=1}^{N}\frac{\chi_{di}(E)}{4\pi}\lambda_i C_i(r,t) + \int_{4\pi} d\Omega' \int_0^{\infty} dE'\ \Sigma_s(r,E'\to E,\hat{\Omega}'\to\hat{\Omega},t)\,\psi(r,E',\hat{\Omega}',t)$$
$$+ s(r,E,\hat{\Omega},t) \qquad (1)$$

Where:

- $\frac{1}{v(E)}\frac{\partial\psi(r,E,\hat{\Omega},t)}{\partial t}$ = neutron flux density with respect to time
    - $v(E)$ = neutron velocity with respect to neutron energy E
    - $\psi(r,E,\hat{\Omega},t)$ = angular neutron flux with respect to volume r, neutron energies E, solid angle $\hat{\Omega}$, and time t
- $\hat{\Omega}\cdot\nabla\psi(r,E,\hat{\Omega},t)$ = neutron leakage rate
    - ∇ = divergence = $\left(\frac{\partial}{\partial x},\frac{\partial}{\partial y},\frac{\partial}{\partial z}\right)$

- $\Sigma_t(r,E,t)\ \psi\left(r,E,\widehat{\Omega},t\right)$ = total neutron collision rate
    - $\Sigma_t(r,E,t)$ = macroscopic total cross section = $\mathcal{N}(r,t)\ \sigma_t(r,E,t)$
        - $\mathcal{N}(r,t)$ = atom density of the material = $\frac{N_A\ \rho(r,t)}{M}$
        - N_A = Avogadro's constant
        - $\rho(r,t)$ = material density
        - M = material molar mass
- $\frac{\chi_p(E)}{4\pi}\int_{4\pi}d\Omega'\int_0^\infty dE'\ \upsilon_p(E')\ \Sigma_f(r,E',t)\ \psi\left(r,E',\widehat{\Omega}',t\right)$ = prompt fission neutron generation rate
    - $\chi_p(E)$ = prompt fission neutron energy distribution
    - E' = incident neutron energy
    - $\upsilon_p(E')$ = average number of neutrons per fission
    - $\Sigma_f(r,E',t)$ = fission macroscopic cross section
- $\sum_{i=1}^{N}\frac{\chi_{di}(E)}{4\pi}\lambda_i C_i(r,t)$ = delayed neutron generation rate
    - $\chi_{di}(E)$ = delayed neutron energy distribution
    - λ_i = decay constant for precursor i
    - $C_i(r,t)$ = total number of precursor i
- $\int_{4\pi}d\Omega'\int_0^\infty dE'\ \Sigma_s\left(r,E'\rightarrow E,\widehat{\Omega}'\rightarrow\widehat{\Omega},t\right)\psi\left(r,E',\widehat{\Omega}',t\right)$ = scattering neutron rate
    - $\Sigma_s\left(r,E'\rightarrow E,\widehat{\Omega}'\rightarrow\widehat{\Omega},t\right)$ = macroscopic scattering cross section for neutrons with respect to volume r, for neutrons scattering from incident energy E' to energy E, in incident solid angle $\widehat{\Omega}'$ to solid angle $\widehat{\Omega}$, time t
- $s\left(r,E,\widehat{\Omega},t\right)$ = source neutron generation rate; external source

There are neutron transport equation introduces several new variables that are important for understanding nuclear systems. First is the angular neutron flux, $\psi(r, E, \hat{\Omega}, t)$. To conceptually understand this term, it is useful to visualize a differential volume $dr = dx \times dy \times dz$ in the cartesian coordinate system. The angular neutron flux, $\psi(r, E, \hat{\Omega}, t)$, in this differential volume, is the sum of the neutron track lengths of differential neutron energies dE, in a differential time span dt, heading in the direction of differential solid angle $d\Omega$.

Another important variable that is introduced in the neutron transport equation is the prompt fission neutron energy distribution, $\chi_p(E)$, which describes the at what energy fission neutrons tend to be born. This distribution can be approximated by the Watt distribution, which is plotted in Figures 3.2 and 3.3 below and visualized with Python's Matplotlib [24, 25].

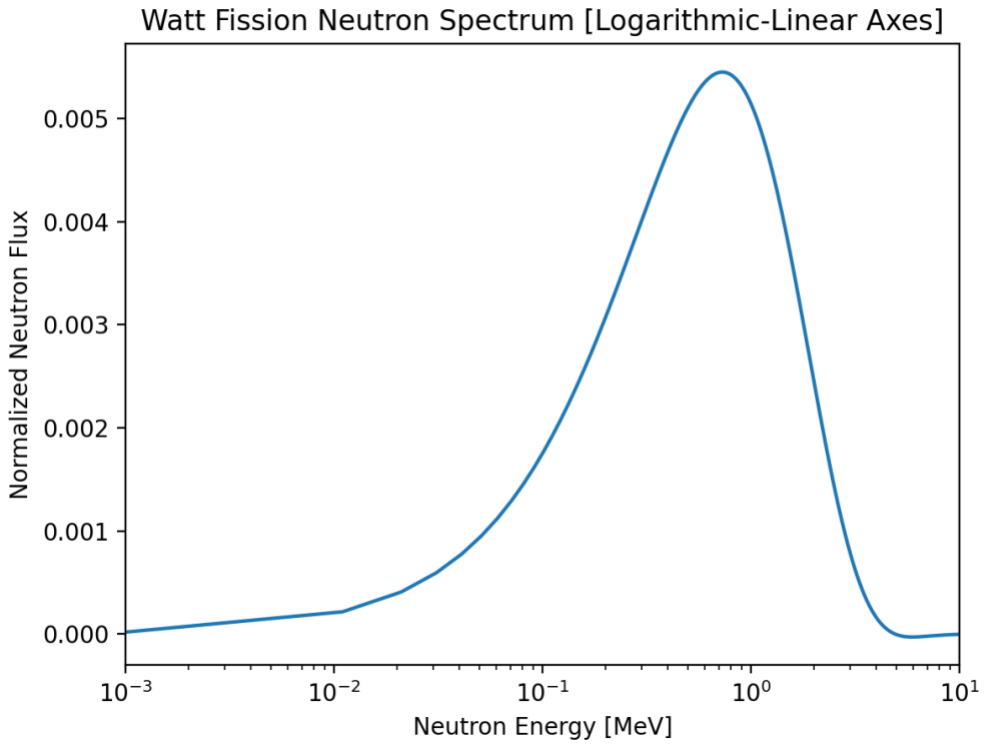

Figure 3.2. Watt fission neutron spectrum on a logarithm-linear axis

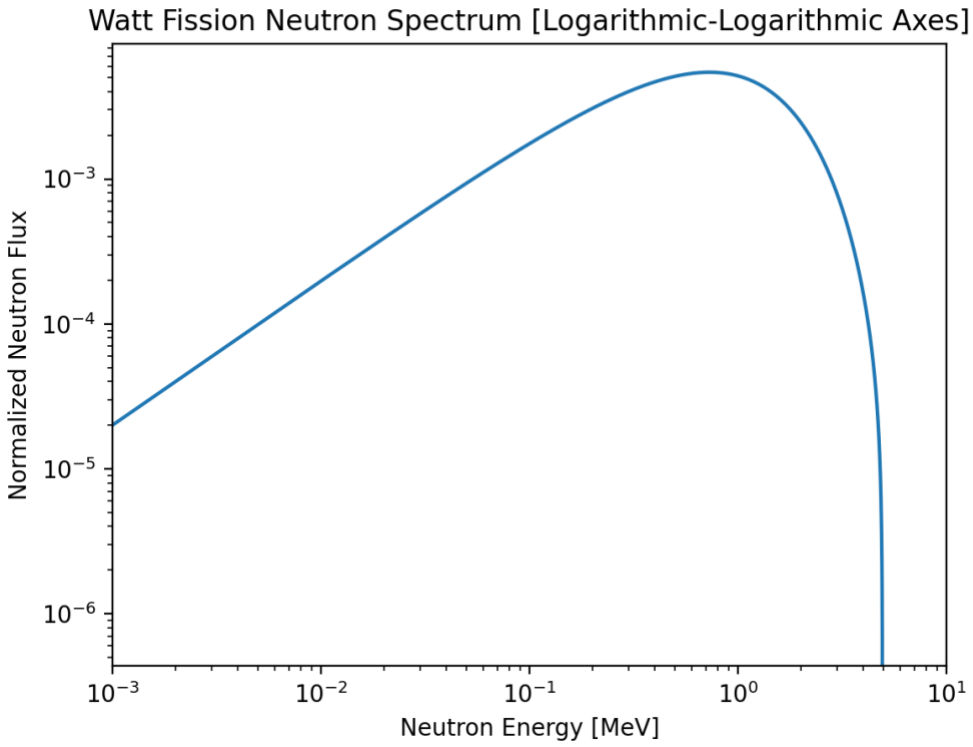

Figure 3.3. Watt fission neutron spectrum on a logarithm-logarithm axis

The fission neutron spectra, for both prompt and delayed neutrons, reveal that most neutrons are born fast (greater than 100 keV). This fact is essential in understanding nuclear systems; it takes additional work to design a nuclear system that efficiently thermalizes neutrons.

The neutron transport equation can be simplified to a time-independent (steady-state), no source equation as seen in Equation (2):

$$\hat{\Omega} \cdot \nabla\psi(r, E, \hat{\Omega}) + \Sigma_t(r, E)\, \psi(r, E, \hat{\Omega})$$

$$= \frac{1}{k}\frac{\chi(E)}{4\pi}\int_{4\pi} d\Omega' \int_0^{\infty} dE'\ \nu(E')\, \Sigma_f(r, E')\, \psi(r, E', \hat{\Omega}')$$

$$+ \int_{4\pi} d\Omega' \int_0^{\infty} dE'\ \Sigma_s(r, E' \to E, \hat{\Omega}' \to \hat{\Omega})\, \psi(r, E', \hat{\Omega}')$$

(2)

Note that a new term, k, has been introduced. The term k is the multiplication factor and is meant to balance the two sides of the equation. This will conceptually make sense when the equation is rearranged by subtracting the neutron scattering rate from both sides as shown in Equation (3). Since $\Sigma_t = \Sigma_a + \Sigma_s$, we can extract the neutron absorption rate by subtracting the scattering rate from the total collision rate term.

$$\hat{\Omega} \cdot \nabla\psi(r, E, \hat{\Omega}) + \int_{4\pi} d\Omega' \int_0^{\infty} dE'\, \Sigma_a(r, E')\, \psi(r, E', \hat{\Omega}')$$

$$= \frac{1}{k}\frac{\chi(E)}{4\pi}\int_{4\pi} d\Omega' \int_0^{\infty} dE'\ \nu(E')\, \Sigma_f(r, E')\, \psi(r, E', \hat{\Omega}')$$

(3)

Where:

- $\int_{4\pi} d\Omega' \int_0^{\infty} dE'\ \Sigma_a(r, E')\, \psi(r, E', \hat{\Omega}')$ = absorption neutron rate
    - $\Sigma_a(r, E') =$ macroscopic absorption cross section for neutrons with respect to volume r, for neutrons of incident energy E'

The left side of this form of the equation represents the neutron losses in the system i.e. the neutron leakage rate term plus the neutron absorption rate term. The right side of the equation

represents the neutron gains in the system i.e. the neutron fission rate term. The losses and gains of a system will not always be equivalent; a nuclear reactor can be subcritical (neutron losses greater than neutron gains) or supercritical (neutron gains greater than neutron losses). Hence, a balancing term, such as the multiplication factor k, is required. Note that if the system is subcritical ($k < 1$), then the right side of the equation is increased to balance the equation. The same is true when the system is supercritical ($k > 1$); the right side of the equation is decreased to match the left side. If the system is perfectly critical ($k = 1$), then the losses equal the gains; the equations are balanced.

The equation can be rearranged to solve for the multiplication factor, k, as shown in Equation (4).

$$k = \frac{\frac{\chi(E)}{4\pi}\int_{4\pi} d\Omega' \int_0^\infty dE'\ \nu(E')\,\Sigma_f(r,E')\,\psi\left(r,E',\widehat{\Omega}'\right)}{\widehat{\Omega}\cdot\nabla\psi\left(r,E,\widehat{\Omega}\right) + \int_{4\pi} d\Omega' \int_0^\infty dE'\,\Sigma_a(r,E')\,\psi\left(r,E',\widehat{\Omega}'\right)} \quad (4)$$

Conceptually, this tells us the multiplication factor is the ratio of the neutron fission rate (gains) and the neutron loss rate (losses). Equation Y can also be conveyed in operator notation as shown in Equation (5).

$$\boldsymbol{M}\psi = k^{-1}\boldsymbol{F}\psi \quad (5)$$

Where $\boldsymbol{M}$ represents the neutron loss operator and $\boldsymbol{F}$ represents the integral fission operator or neutron gain operator. This operator notation will be useful when delving into first-order perturbation theory and deriving the adjoint-based sensitivity coefficient.

Section 3.3. Sensitivity Coefficients and First-Order Perturbation Theory

Sensitivity coefficients, $S_{k,x}$, describe the sensitivity of a system's effective multiplication factor, k_{eff}, to a perturbation of nuclear data, x, at all incident neutron energies, E'. Sensitivity coefficients are defined via equation (6).

$$S_{k,x} = \frac{x}{k}\frac{\partial k}{\partial x} \tag{6}$$

Conceptually, the stochastic sensitivity coefficient can be understood by example and by inserting a nuclear data parameter in place of x, such as the fission cross section σ_f. For example, a small change in σ_f due to a small reactivity insertion that leads to a large change in the multiplication factor, k, would lead to a large sensitivity coefficient, i.e., the system is sensitive and strongly affected by a change in the fission cross section. The inverse is also true; a large change in σ_f with a small change in k would lead to a small sensitivity coefficient i.e. the system is insensitive to changes to the material property.

The stochastic sensitivity coefficient is, in theory, a robust method to generate sensitivity coefficients. However, the stochastic method is computationally expensive since a simulation would need to be conducted for every nuclear data parameter. An alternative way to accurately estimate the sensitivity coefficient is possible via first-order perturbation theory.

The following derivation will demonstrate how first-order perturbation theory can estimate the sensitivity coefficient. First-order perturbation theory in neutronics studies the first-order effects of small changes to a system. When taking a look at the variables from the neutron transport equation in operator form, this translates to the set of equation (7) below:

$$\psi = \psi_0 + \Delta\psi \cancel{+ (\Delta\psi)^2 + \cdots}$$

$$\boldsymbol{M} = \boldsymbol{M_0} + \Delta\boldsymbol{M} \cancel{+ (\Delta\boldsymbol{M})^2 + \cdots}$$

$$k^{-1} = k_0^{-1} + \Delta k^{-1} \cancel{+ (\Delta k)^2 + \cdots}$$

$$\boldsymbol{F} = \boldsymbol{F_0} + \Delta\boldsymbol{F} \cancel{+ (\Delta\boldsymbol{F})^2 + \cdots}$$

(7)

Where ψ is the perturbed neutron flux, ψ_0 is the unperturbed neutron flux, $\Delta\psi$ is the first-order change in neutron flux, $\Delta\psi^2$ is the second-order change in neutron flux, $\boldsymbol{M}$ is the perturbed neutron loss operator, $\boldsymbol{M_0}$ is the unperturbed neutron loss operator, $\Delta\boldsymbol{M}$ is the first-order change in neutron loss operator, $\Delta\boldsymbol{M^2}$ is the second-order change in neutron loss operator, $\boldsymbol{k}$ is the perturbed multiplication factor, k_0 is the unperturbed multiplication factor, Δk is the first-order change in the multiplication factor, Δk^2 is the second-order change multiplication factor, F is the perturbed neutron gain operator, $\boldsymbol{F_0}$ is the unperturbed neutron gain operator, $\Delta\boldsymbol{F}$ is the first-order change in neutron gain operator, and $\Delta\boldsymbol{F^2}$ is the second-order change in neutron gain operator. Note that the second-order and higher effects of each definition are neglected due to the first-order approximation.

Now that we have the definitions for the perturbed terms, we can define the perturbed and unperturbed forms of the neutron transport equation in operator notation in equation (8).

$$\boldsymbol{M}\psi = k^{-1}\boldsymbol{F}\psi$$

$$\boldsymbol{M_0}\psi_0 = k_0^{-1}\boldsymbol{F_0}\psi_0$$

(8)

By expanding the perturbed neutron transport equation in operator notation, we get equation (9):

$$(\boldsymbol{M_0} + \Delta\boldsymbol{M})(\psi_0 + \Delta\psi) = (k_0^{-1} + \Delta k^{-1})(\boldsymbol{F_0} + \Delta\boldsymbol{F})(\psi_0 + \Delta\psi)$$

(9)

Further expanding the equation leads to second-order terms that are able to be eliminated due to the first-order approximation as seen in the equations (10) below.

$$\boldsymbol{M_0}\psi_0 + \boldsymbol{M_0}\Delta\psi + \Delta\boldsymbol{M}\psi_0 \cancel{+ \Delta\boldsymbol{M}\Delta\psi} = (k_0^{-1}\boldsymbol{F_0} + k_0^{-1}\Delta\boldsymbol{F} + \Delta k^{-1}\boldsymbol{F_0} \cancel{+ \Delta k^{-1}\Delta\boldsymbol{F}})\ (\psi_0 + \Delta\psi)$$

$$\boldsymbol{M_0}\psi_0 + \boldsymbol{M_0}\Delta\psi + \Delta\boldsymbol{M}\psi_0 = k_0^{-1}\boldsymbol{F_0}\psi_0 + k_0^{-1}\Delta\boldsymbol{F}\psi_0 + \Delta k^{-1}\boldsymbol{F_0}\psi_0 + k_0^{-1}\boldsymbol{F_0}\Delta\psi \cancel{+ k_0^{-1}\Delta\boldsymbol{F}\Delta\psi} + \cancel{\Delta k^{-1}\boldsymbol{F_0}\Delta\psi}$$

(10)

By taking the definition of the unperturbed neutron transport equation, the equation can be further reduced to equation (11) below:

$$\cancel{\boldsymbol{M_0}\psi_0} + \boldsymbol{M_0}\Delta\psi + \Delta\boldsymbol{M}\psi_0 = \cancel{k_0^{-1}\boldsymbol{F_0}\psi_0} + k_0^{-1}\Delta\boldsymbol{F}\psi_0 + \Delta k^{-1}\boldsymbol{F_0}\psi_0 + k_0^{-1}\boldsymbol{F_0}\Delta\psi$$

(11)

Shifting the terms leads to equation (12).

$$-\Delta k^{-1}\boldsymbol{F_0}\psi_0 = (k_0^{-1}\Delta\boldsymbol{F} - \Delta\boldsymbol{M})\psi_0 + (k_0^{-1}\boldsymbol{F_0} - \boldsymbol{M_0})\Delta\psi$$

(12)

In order to further manipulate the equations, the property of adjoints will be utilized as shown in equation (13) below. The properties of adjoints will play an important role in eliminating the change in perturbed flux term, $\Delta\psi$, which is typically an expensive computation.

$$\langle\psi^\dagger, \boldsymbol{F}\psi\rangle = \langle\psi, \boldsymbol{F}^\dagger\psi^\dagger\rangle$$

(13)

Where $\psi^\dagger$ is the adjoint neutron flux, $\boldsymbol{F}^\dagger$ is the adjoint neutron gain operator, and $\langle *,* \rangle$ denotes an inner product. Mathematical operators have adjoints that must satisfy this property; adjoints can be the term itself (self-adjoint), a negative of a derivative term, a transpose of a real matrix, etc. as long as the definition in equation 13 is satisfied. This leads to the adjoint neutron transport equation as shown in equation (14) [26]:

$$\boldsymbol{M}^\dagger\psi^\dagger = k^{-1}\boldsymbol{F}^\dagger\psi^\dagger$$

(14)

Note that the multiplication factor is self-adjoint as shown in equation (15).

$$\frac{1}{k}^\dagger = \frac{1}{k}$$

(15)

A conceptual interpretation of the adjoint flux in neutronics is that the adjoint flux represents the neutron "importance," i.e., how consequential the neutron is to the overall system. The conceptual interpretation is often paired with the interpretation of the adjoint neutron

transport simulation as a "backward simulation." This interpretation makes more sense when understanding how MCNP calculates the adjoint flux via the Iterated Fission Probability method [27].

The iterated fission probability method tracks neutrons and their "generations" i.e. neutrons born from the "parent" neutron. After several generations and the fundamental mode of the neutron flux is converged, the fraction of current generation neutrons that arose due to the first-generation neutron dictates the "importance" of that neutron. Neutrons that led to a large percentage of present generation neutrons are more important than neutrons that leaked entirely after a generation or two. MCNP uses this method to calculate the adjoint flux. Since MCNP is already generating the data of neutron histories, the biggest computational cost to the method is storing the information of several neutron generations in memory. MCNP employs the iterated fission probability method via the KSEN input line.

The adjoint can further be explained by taking a look at the explicit definitions of the neutron leakage terms as seen in equations (16).

$$\boldsymbol{M_{leak}}\ \psi = \widehat{\Omega} \cdot \nabla\psi\left(r, E, \widehat{\Omega}\right)$$

$$\boldsymbol{M_{leak}^{\dagger}}\ \psi^{\dagger} = -\widehat{\Omega} \cdot \nabla\psi^{\dagger}\left(r, E, \widehat{\Omega}\right) \qquad (16)$$

The standard definition for neutron leakage conceptually represents the neutrons diffusing away from regions of high neutron concentration and will, accordingly, leak out of the boundaries per the positive divergence term. The lack of neutrons leads to neutrons being added to the region. The adjoint definition is the opposite; the lack of neutrons in the region will lead to

neutron importance dropping in the region as denoted by the negative sign. Conceptually, this makes sense; neutrons in high concentration regions tend to be in the center of the reactor system and will most likely have several generations contributing to the present neutron flux; neutrons close to the boundary, i.e., lower importance regions, have a higher chance of leaking and hence contributing less to the present neutron flux.

The adjoint for the leakage term was a simple negative term, but as stated earlier, an adjoint can be the transpose of a matrix, as shown in equations (17) for the neutron scattering term.

$$\boldsymbol{M}_{\boldsymbol{scatter}}\,\psi = \int_{4\pi} d\Omega' \int_0^{\infty} dE'\ \Sigma_s\left(r, E' \rightarrow E, \widehat{\Omega}' \rightarrow \widehat{\Omega}\right) \psi\left(r, E', \widehat{\Omega}'\right)$$

$$\boldsymbol{M}^{\dagger}_{\boldsymbol{scatter}}\,\psi^{\dagger} = \int_{4\pi} d\Omega' \int_0^{\infty} dE'\ \Sigma_s\left(r, E \rightarrow E', \widehat{\Omega} \rightarrow \widehat{\Omega}'\right) \psi^{\dagger}\left(r, E', \widehat{\Omega}'\right) \quad (17)$$

Normally, the scattering term cares about the incident neutron energy E' which affects the macroscopic scattering cross section, Σ_s and the likelihood of scattering into final energy E. The adjoint scattering term is backwards; the adjoint term is interested in the final neutron energy, E, and the likelihood that it was scattered from some incident neutron energy, E'. The same applies to the incident solid angle variable.

Returning to the first-order perturbation neutron transport equations, we can take advantage of the properties of adjoints via equation (18) by multiplying equation (12) with the unperturbed adjoint neutron flux and taking the inner product.

$$-\Delta k^{-1}\langle \psi_0^\dagger, \boldsymbol{F_0}\psi_0\rangle = \langle \psi_0^\dagger,\ (k_0^{-1}\Delta \boldsymbol{F} - \Delta \boldsymbol{M})\psi_0\rangle + \langle \psi_0^\dagger,\ (k_0^{-1}\boldsymbol{F_0} - \boldsymbol{M_0})\Delta\psi\rangle$$

(18)

By utilizing the properties of adjoints, we find that the highlighted portion of the previous equation is equivalent to equation (19):

$$\langle \psi_0^\dagger,\ (k_0^{-1}\boldsymbol{F_0} - \boldsymbol{M_0})\Delta\psi\rangle = \langle \Delta\psi,\ (k_0^{-1}\boldsymbol{F_0^\dagger} - \boldsymbol{M_0^\dagger})\psi_0^\dagger\rangle$$

(19)

Per the definition of the unperturbed adjoint neutron transport equation, the highlighted portion is equivalent to zero as seen in equation (20) which leads to equation (21).

$$\boldsymbol{M_0^\dagger}\psi_0^\dagger = k_0^{-1}\boldsymbol{F_0^\dagger}\psi_0^\dagger$$

(20)

$$-\Delta k^{-1}\langle \psi_0^\dagger, \boldsymbol{F_0}\psi_0\rangle = \langle \psi_0^\dagger,\ (k_0^{-1}\Delta \boldsymbol{F} - \Delta \boldsymbol{M})\psi_0\rangle$$

(21)

Solving $-\Delta k^{-1}$ yields equations (22) [27]:

$$-\Delta k^{-1} = \frac{\langle \psi_0^\dagger, (k_0^{-1}\Delta \boldsymbol{F} - \Delta \boldsymbol{M})\psi_0\rangle}{\langle \psi_0^\dagger, \boldsymbol{F_0}\psi_0\rangle}$$

$$\Delta k = -\frac{\langle \psi_0^\dagger, (\Delta \boldsymbol{M} - k_0^{-1}\Delta \boldsymbol{F})\psi_0\rangle}{\langle \psi_0^\dagger, \boldsymbol{k_0^{-2}F_0}\psi_0\rangle}$$

(22)

We can take the differential with respect to the change in material property, Σ_x, of the change in reactivity to get equation (23):

$$\frac{\partial k}{\partial x} = -\frac{\left\langle \psi_0^{\dagger}, (\frac{\partial \boldsymbol{M}}{\partial \Sigma_x} - k_0^{-1}\frac{\partial \boldsymbol{F}}{\boldsymbol{d\Sigma_x}})\psi_0 \right\rangle}{\left\langle \psi_0^{\dagger}, \boldsymbol{k_0^{-2} F_0} \psi_0 \right\rangle}$$

(23)

Multiplying by the ratio of the material property and the multiplication factor yields equation (24):

$$S_{k,x} = \frac{x}{k}\frac{\partial k}{\partial x} \cong -\frac{\Sigma_x \left\langle \psi_0^{\dagger}, (\frac{\partial \boldsymbol{M}}{\partial \Sigma_x} - k_0^{-1}\frac{\partial \boldsymbol{F}}{\boldsymbol{d\Sigma_x}})\psi_0 \right\rangle}{\left\langle \psi_0^{\dagger}, \boldsymbol{k_0^{-1} F_0} \psi_0 \right\rangle}$$

(24)

This derived definition of the sensitivity coefficient from first-order perturbation theory is can be further manipulated to match the MCNP estimation of the sensitivity coefficient as shown in equation (25) which uses the iterated fission probability method [28].

$$S_{k,x} \cong -\frac{\langle \psi^{\dagger}, (\Sigma_x - \mathcal{K}_x - k^{-1}\mathcal{F}_x)\, \psi \rangle}{\langle \psi^{\dagger},\ \mathcal{F}\psi \rangle}$$

(25)

Where $\psi^{\dagger}$ is the adjoint flux, $\mathcal{F}$ is the fission operator of the whole system, ψ is the flux, $\langle *,* \rangle$ denotes an inner product, Σ_x is the macroscopic interaction, $\mathcal{K}_x$ is the scattering operator, and $\mathcal{F}_x$ is the fission operator of nuclear data x. This definition is how MCNP calculates the sensitivity coefficient via the KSEN input line. The adjoint-based sensitivity coefficient is an accurate approximation when uncertainty in nuclear data is low and the perturbation made on the data is small.

Section 3.4. Correlation Coefficients and Whisper

When comparing the neutronic similarity between two systems, sensitivity coefficients are essential, since they will provide the sensitivity to nuclear data over all incident neutron energies. Another important characteristic when comparing to nuclear systems is the amount of shared nuclear data uncertainty. A method of folding together both the sensitivity coefficients and the nuclear data uncertainty is the correlation coefficient for the effective multiplication factor as defined in equation (26) with the covariance with respect to multiplication factor defined in equation (27).

$$c_k(A,B) = \frac{Cov_k(A,B)}{\sqrt{Var_k(A)}\sqrt{Var_k(B)}} \quad (26)$$

$$Cov_k(A,B) = S_A C_{xx} S_B^T \quad (27)$$

Where $Cov_k(A,B)$ is the covariance in the multiplication factor, k, for some two systems A and B, S_A and S_B^T are the sensitivity row vectors of systems A and B respectively, C_{xx} is the nuclear data relative covariance matrix, T is the transpose operator, $c_k(A,B)$ is the correlation coefficient for some two systems A and B, and $Var_k(A)$ and $Var_k(B)$ are the variance in the multiplication factor, k, for systems A and B respectively.

Whisper generates the correlation coefficients for a system with sensitivity coefficients generated from MCNP and existing benchmark experiments. Whisper sets negative correlations to zero, meaning c_k can range from zero to one. A correlation of one, or 100%, is a perfect correlation and systems A and B would have identical sources of bias. As a rule of thumb, the

two systems should have a correlation coefficient of at least 0.80 to be considered neutronically similar with regards to their sources of biases [29].

By folding both the sensitivity coefficients and the nuclear data uncertainty, correlation coefficients are a robust method of comparing the neutronics of two systems. Conceptually, the correlation coefficient is the ratio of shared uncertainty in the multiplication factor between two nuclear systems. The correlation coefficient is particularly useful for guiding the design of an experiment. This can be done in Whisper by adding the full-scale nuclear reactor as a custom benchmark; any experiment design run through Whisper will get a correlation coefficient generated against the full-scale nuclear reactor. If an experiment for a microreactor is designed to maximize the correlation coefficient, then this means that any discrepancy between the modeling and simulation of the experiment and the experiment data will give insights on any potential discrepancy when modeling and simulating the full-scale microreactor system.

Chapter 4 - Methodology

Section 4.1. Experimental Facility

To conduct a nuclear experiment, a facility that has existing safety basis authorization, procedures, and critical assemblies with trained personnel in place will be necessary. In order to create a model that takes experimental limitations into account, the National Criticality Experiments Research Center is chosen as the potential site to conduct these conceptual experiments. Taking into account realistic experimental conditions is necessary to ground conceptual models to reality and increase the likeliness of the model becoming a reality.

At the National Criticality Experiments Research Center, a precise vertical lift machine known as Comet is particularly well suited for microreactor experiments. Comet has a static structure with a platen in the center that moves up and down at precise intervals sensitive enough to slowly insert reactivity into a nuclear system as seen in Figure 4.1 [30].

Figure 4.1. Comet machine at the National Criticality Experiments Research Center [30]

As with any facilities, there are limitations that the MCNP models will have to take into account. These limitations include but are not limited to:

- Machine weight limitations for the platen (<2,000 pounds) and the structure (<20,000 pounds)
- Machine size limitations
- Room size/dimensions
- Maximum effective multiplication factor when the experiment is in the subcritical configuration
- Activation of the structure and the room

As a result of these limitations, nuclear experiments will have a much smaller space to operate in compared to their full-scale reactor counterparts. The smaller volume may necessitate the use of higher-enriched fuel to ensure sufficient reactivity is present.

The smaller space and the use of higher-enriched fuel poses an important question: how do we know if the two systems are neutronically similar? After all, the higher-enriched fuel will interact differently with the neutrons of the system; a smaller volume will be more prone to neutron leakage. Correlation coefficients are one objective way to assess the neutronic similarity at all incident neutron energies between two systems and should be included in conjunction with other neutronic analyses.

Section 4.2. Proposed Microreactor Experiments

Several microreactor experiment designs are constructed in MCNP with two main intentions. First, to maximize the correlation coefficient generated with Whisper. Second, to study the effects of different configurations/materials on the correlation coefficient and study any patterns with regards to other neutronics characteristics. A single unit cell from the Snowflake core lattice is placed in the center region of the Comet assembly. The Snowflake unit cell is first surrounded by a hexagonal ring of moderator and then by an outer region containing moderator, heat pipes, and highly-enriched fuel in a graphite solid block. The entire experiment is surrounded by beryllium oxide that acts as a neutron reflector; this reflector will be raised up and down with the Comet platen to control reactivity since the experiment will be highly reliant on the neutron reflector as shown in Figure 4.2.

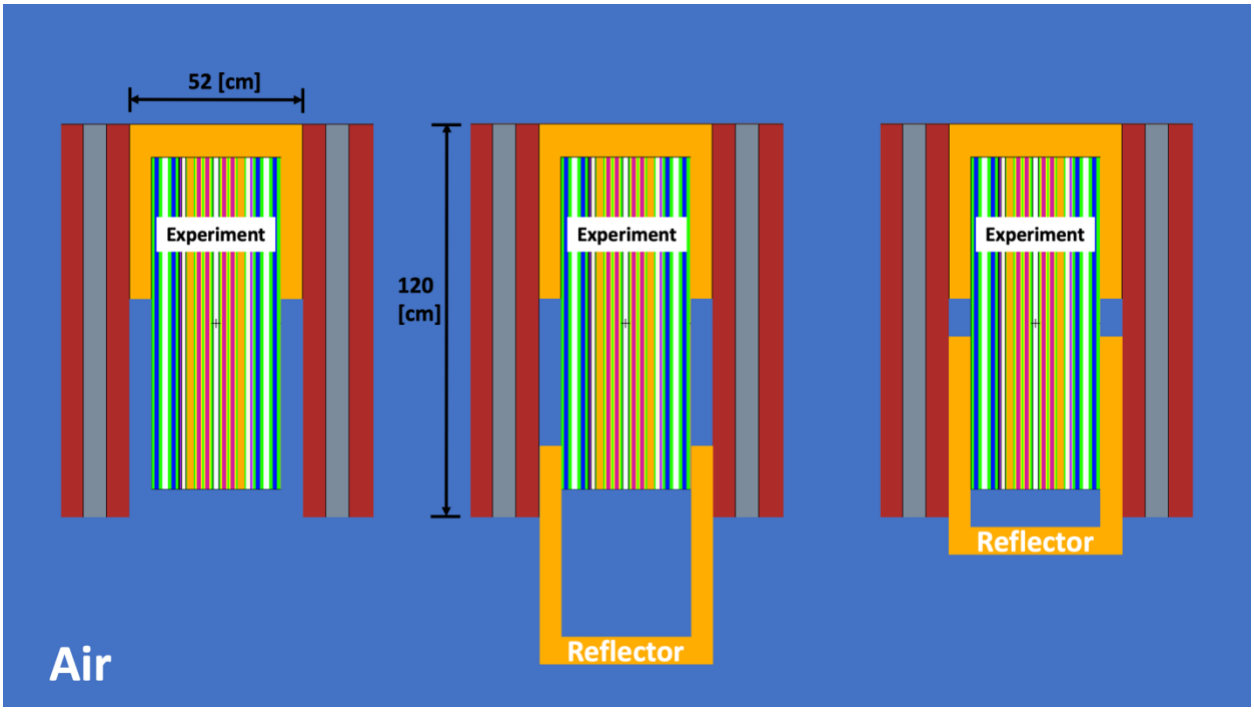

Figure 4.2. Axial view of experiment, reactivity control via movement of reflector [3]

The beryllium oxide removal can serve as a precise reactivity control tool since the platen can move vertically at precise intervals. The reactivity curve for the beryllium oxide reflector can be seen in Figure 4.3. with the reactivity of the system dropping the further the beryllium oxide reflector is withdrawn axially.

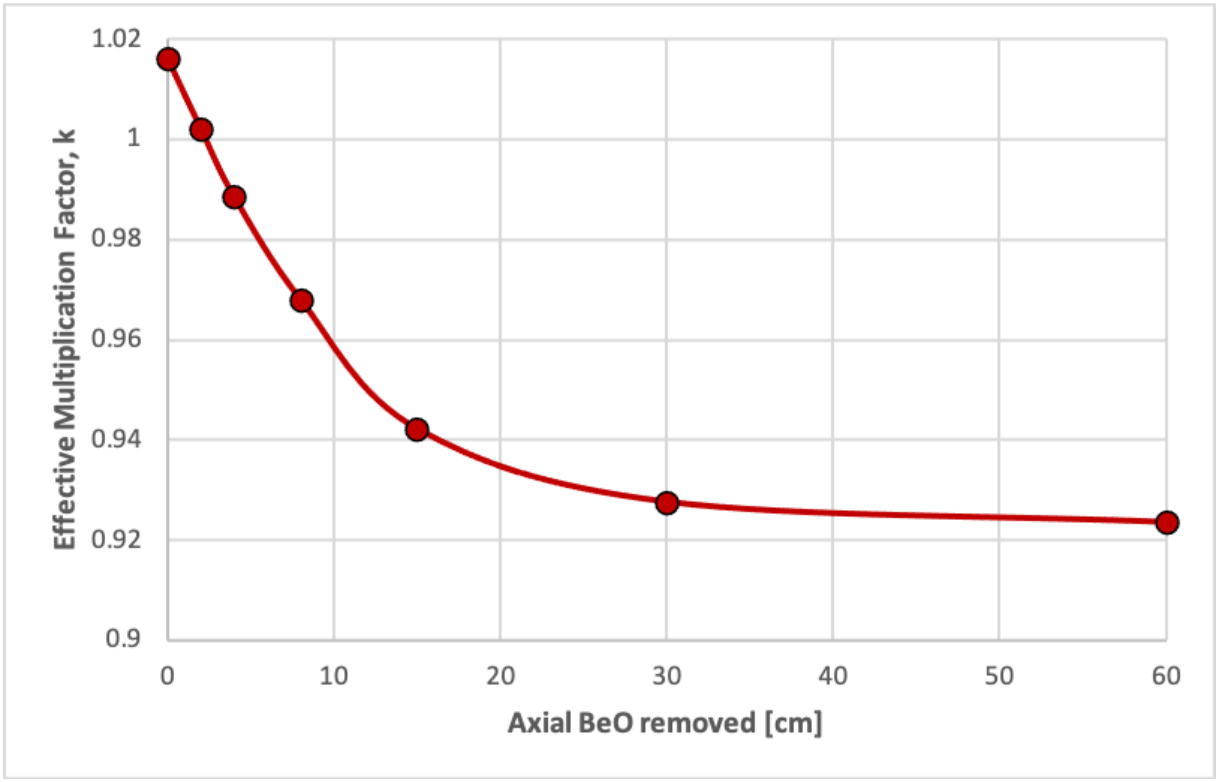

Figure 4.3. Potential effective multiplication factor curve with respect to BeO removed [3, 31]

The goal of placing the Snowflake unit cell in the center region is to ensure the unit cell sees a sizeable share of the neutron flux. Conducting an experiment with the exact unit cell that would be placed in the full-size microreactor may also aid in the licensing process. A limitation to using the exact unit cell in the full-scale microreactor is the lack of flexibility; if the microreactor design is set in stone, this inner region of the experiment also has to stay constant.

Another limitation is that a single Snowflake unit cell does not have sufficient reactivity to go critical by itself. Hence, the outer region could be supplied with highly-enriched uranium nitride to ensure the experiment has sufficient reactivity.

Since the outer region is not particular to any design, the outer region configuration and materials can be varied to maximize the correlation coefficient. The outer region provides a great set-up to study patterns that arise in the neutronics as a result of trying to maximize the correlation coefficient as is explored in this research. Experiment configurations, without the use of highly-enriched fuels, are also being investigated at Los Alamos National Laboratory but they are less flexible in their design due to the lower reactivity that comes from low-enriched uranium fuel and will therefore not be covered in this research.

Experiment v0, as shown in Figure 4.2 below, is the first microreactor experiment design and introduces the yttrium hydride pins in the exterior regions. Since yttrium hydride is the moderator material used in Snowflake, it is also used as a ring around the unit cell and within the outer region to thermalize neutrons from the driver fuel outside the unit cell. The critical experiment could be performed solely at zero power and room temperature; if necessary, facility and safety approvals are obtained, higher temperatures and/or power could be achieved. However, operating even at low power levels involves significant fission events and generation of fission products that lead to radiation doses in the surrounding room. It can take weeks and/or months for radiation doses to decay to levels such that other experiments can be performed in the room, which is not preferable from an experimental standpoint. Thus, heat pipes are present primary for neutronic contribution purposes but could also be used for heat removal, depending on the experiment. Each microreactor experiment is also designed to be a sixth symmetric at the

hexagon faces in case a smaller, reflected model has to be created to reduce computational burden.

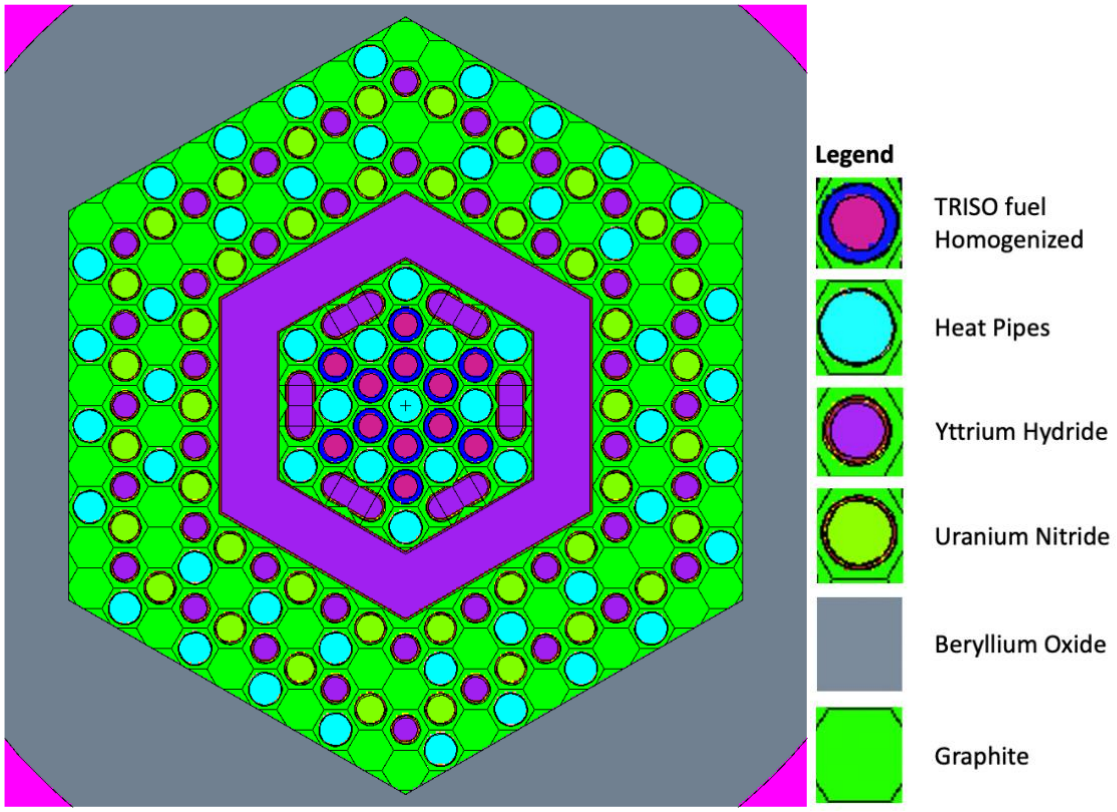

Figure 4.4. Microreactor Experiment v0, MCNP render

Experiment v1, as shown in Figure 4.4, increases the size of the hexagonal ring of yttrium hydride surrounding the unit cell. Additionally, the yttrium hydride pins in the exterior region are also larger in diameter to try to increase the experiment's sensitivity to the yttrium hydride cross sections. Notice that the heat pipes in the outer region were also removed; if low power and/or high temperature experiments are performed, a heat transfer mechanism may be required to cool this outer region. For now, it is assumed that the design is flexible and we are only trying to maximize the correlation coefficient.

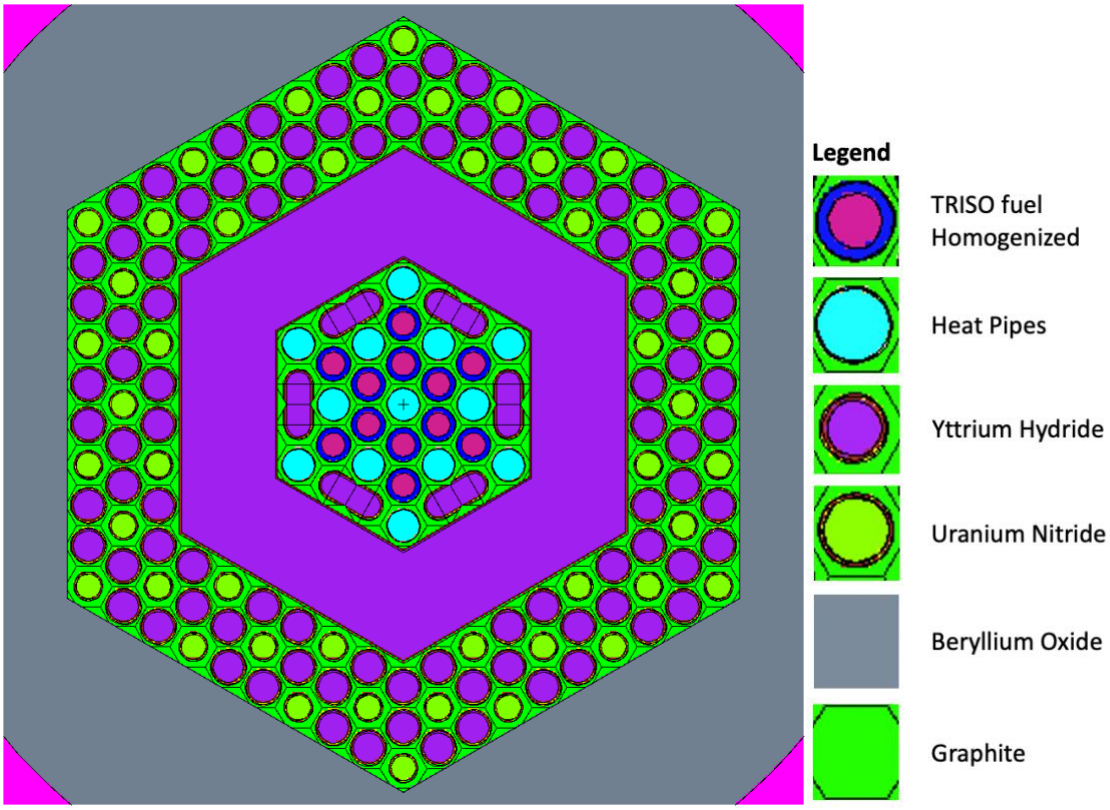

Figure 4.5. Microreactor Experiment v1, MCNP render

Experiment v2, as shown in Figure 4.5, introduces zirconium hydride to the experiment design. Zirconium hydride, for equivalent volume, has a higher reactivity worth than yttrium hydride, but struggles to retain hydrogen past about 500°C - 600°C and thus is not as appealing for efficient microreactor performance. Additionally, zirconium hydride is used in place of the yttrium hydride in the hexagonal ring. The primary reason for using zirconium hydride in place of yttrium hydride in this latest experiment iteration is to increase the number of thermal neutrons causing fission, since the experiments have a lower percentage compared to the full-scale Snowflake microreactor. A gap between the unit cell and the outer region is also introduced; this gap can be used for additional experiment flexibility with regards to thermal heat

transfer considerations. For example, the gap can be used to insert electrical heaters if the experiment wants to measure reactivity impacts of the system at higher temperatures without the need for fission power to heat up the system.

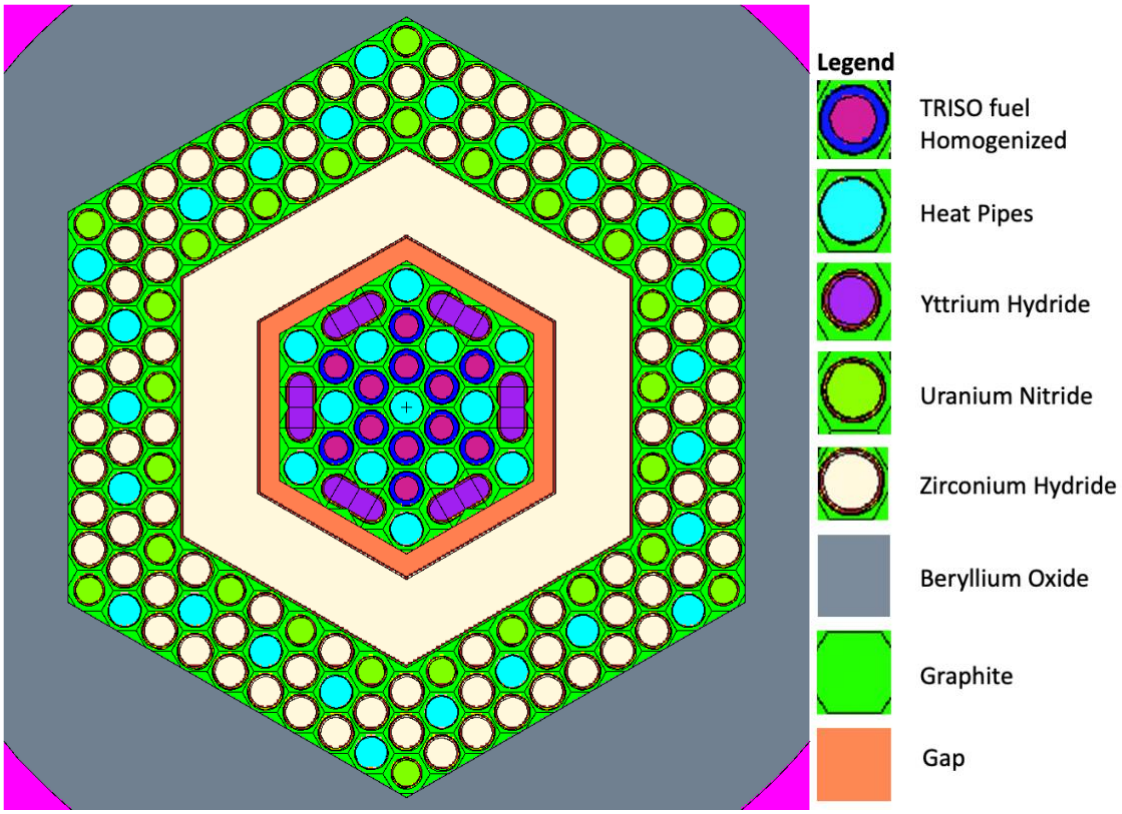

Figure 4.6. Microreactor Experiment v2, MCNP render

The final experiment design, microreactor experiment v3 as shown in Figure 4.5, introduces a second hexagonal ring in the outer region that contains yttrium hydride. The purpose of this hexagonal ring is two-fold. First, the outer hexagonal yttrium hydride ring thermalizes additional neutrons in the outer region and second, it increases the system's sensitivity to yttrium hydride.

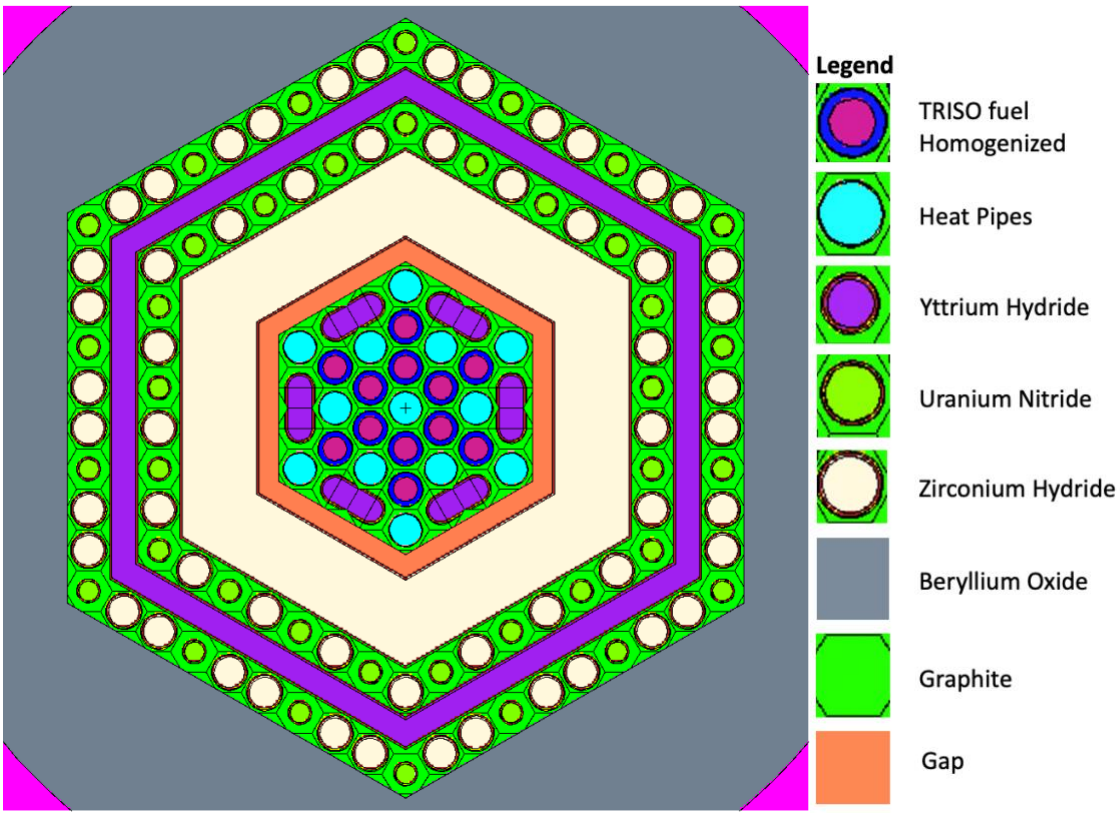

Figure 4.7. Microreactor Experiment v3, MCNP render

Section 4.3. Proposed Analyses

Now that the microreactor experiments have been presented, the question arises: which experiment design is best suited to neutronically represent the full-scale Snowflake microreactor? There are several neutronic characteristics that can be analyzed to make this assessment. The neutronics characteristics that will be analyzed in this research are the percentage of neutron energies (thermal, epithermal, and fast) causing fission, the normalized flux per unit lethargy, the sensitivity coefficients with respect to neutron energy for select materials, and the correlation coefficients.

MCNP will be used to generate the effective multiplication factor and the percentage of neutron energies (thermal, epithermal, and fast) causing fission with the KCODE input line. Understanding the percentage of neutron energies causing fission is essential in understanding how the systems will react to certain materials. For example, under-moderated systems will react differently to the introduction of additional moderator, which will result in an increase in reactivity due to the thermalization of additional neutrons that leads to higher cross sections in fuels, compared to over-moderated systems which will see a drop in reactivity due to additional parasitic absorption from the extra moderator. Furthermore, understanding the neutron energies causing fission will help the analyst understand where the nuclear data uncertainties will play a larger role.

MCNP will calculate the normalized flux per unit lethargy via the F4 tally which will be plotted with Python's Matplotlib library [25, 33]. The normalized flux per unit lethargy will report the share of neutron energies in the nuclear system. The sensitivity coefficients with respect to neutron energy for select materials will also be generated with MCNP via the KSEN input line and will be plotted with Python's Matplotlib. The sensitivity coefficients will provide

valuable information regarding how sensitive the system is to a change in the nuclear data plotted at all incident neutron energy ranges.

Whisper will generate the correlation coefficients for the two systems; this will be done by adding the full-scale Snowflake microreactor as a custom benchmark. Every experiment input into Whisper will then have a correlation coefficient generated for the full-scale Snowflake microreactor. The correlation coefficient will provide the ratio of shared nuclear data uncertainty between the two systems by folding together the two systems' sensitivity coefficients and the nuclear data covariance matrix.

The overall process can be summarized in the following manner:

1. Generate the MCNP input deck for full-scale nuclear system
2. Run the MCNP criticality (KCODE) input deck with k_{eff} sensitivity tallies option (KSEN card)
3. Add full-scale system to Whisper as a Custom Benchmark; see Whisper Manual [5]
4. Test addition of custom benchmark by running the full-scale system as a Whisper input
    a. This should yield a c_k = 1.0, perfect correlation since it is the same system
5. Generate an MCNP input deck for an experiment design
6. Run the MCNP criticality (KCODE) input deck with k_{eff} sensitivity tallies option (KSEN card)
7. Run experiment as Whisper input to generate c_k for experiment and full-scale system

Chapter 5 - Results

Section 5.1. Neutron flux and percentage of neutrons causing fissions analyses

Table I compares the effective multiplication factor, correlation coefficient for k_{eff}, and the percentages of neutron energies causing fission for the Snowflake full-scale microreactor and the four candidate experiment designs. To generate this data, MCNP6.1.4 along with ENDF/B-VIII.0 cross sections with ENDF80SaB2 thermal scattering data. For the correlation coefficients, Whisper1.1 was utilized; it is important to note that Whisper at this time does not have the covariance data for yttrium-hydride.

Table I. Effective multiplication factors, correlation coefficients, and percentages of neutron energies causing fission from MCNP and Whisper

System	Effective Mult. Factor, k_{eff}	Corr. Coeff. %, c_k	% of neutrons causing fission (E < 0.625 eV)	% of neutrons causing fission (0.625 eV < E < 100 keV)	% of neutrons causing fission (100 keV < E)
Experiment v0	1.02312	65.91%	39.20%	43.81%	16.99%
Experiment v1	1.01485	75.90%	48.20%	37.21%	14.60%
Experiment v2	1.00567	86.55%	60.07%	29.09%	10.84%
Experiment v3	1.00338	90.31%	66.66%	25.45%	7.89%
Unit-Level Microreactor	**1.07946**	-	**83.37%**	**14.98%**	**1.64%**

Table II compares the average neutron energy causing fission and the energy corresponding to average neutron lethargy causing fission, both metrics useful for characterizing spectrum hardness. The lower these values are, the more thermal the spectrum.

Table II. Effective multiplication factors, correlation coefficients, average neutron energy causing fission and energy corresponding to average neutron lethargy causing fission

System	Effective Mult. Factor, k_{eff}	Corr. Coeff. %, c_k	Average Neutron Energy Causing Fission [MeV]	Energy corresponding to the Average neutron Lethargy causing Fission [MeV]
Experiment v0	1.02312	65.91%	2.4750E-01	4.3319E-05
Experiment v1	1.01485	75.90%	2.2479E-01	1.6680E-05
Experiment v2	1.00567	86.55%	1.7412E-01	4.7322E-06
Experiment v3	1.00338	90.31%	1.2888E-01	2.1966E-06
Unit-Level Microreactor	**1.07946**	-	3.2317E-02	2.8491E-07

When studying Table I, an interesting trend arises; with increasing correlation coefficient for the microreactor experiments, the percentage of neutrons causing fission in each energy group is converging to the results of the unit-level (full-scale) Snowflake microreactor concept. Intuitively, this makes sense since neutrons causing fission will play a large role in the overall neutronics of a system; these neutrons are particularly affected by any uncertainty present in the uranium cross section data, which is factored into the correlation coefficient along with the

sensitivity coefficients. Table II further supports this trend; both the average neutron energy causing fission and the average neutron lethargy causing fission are converging towards the full-scale microreactor values with increasing correlation coefficient.

Figure 5.1 plots the normalized flux per unit lethargy with respect to the neutron energy for the microreactor experiments and the unit-level Snowflake microreactor [34].

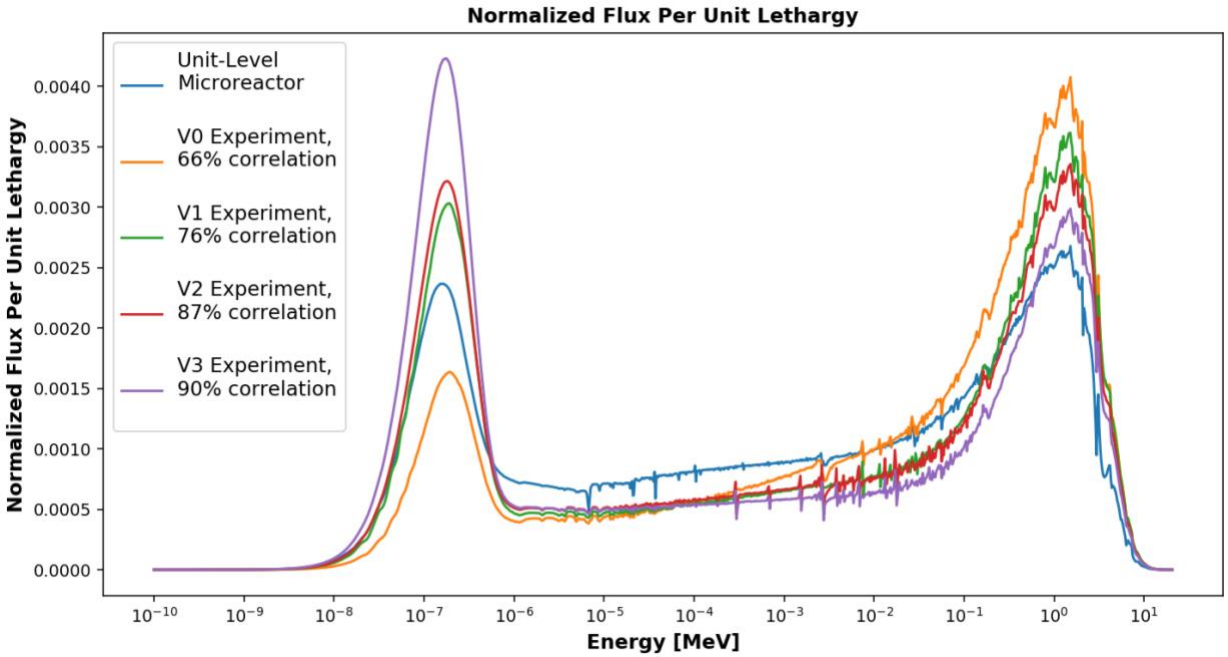

Figure 5.1. Normalized flux per unit lethargy with respect to neutron energy

As shown in Figure 5.1, with increasing correlation coefficients for the microreactor experiments, the share of thermal neutrons also increases, even past the share of thermal neutrons present in the Snowflake microreactor. This is interesting because the percentage of thermal neutrons causing fission is highest in the Snowflake microreactor concept, but the thermal neutron hill in the plot is the second lowest. On the right side, the fast neutron hill shows the opposite trend as the thermal neutron hill; with increasing correlation coefficients, the

microreactor experiments fast neutron share decreases and converges towards the Snowflake microreactor fast neutron share. This makes sense, since the percentage of fast neutrons causing fission consistently drops with increasing correlation coefficient per Table I.

There are two potential factors that explain the increase in share of thermal neutrons and the decrease in share of fast neutrons with increasing correlation coefficients for the microreactor experiments. These factors are first, the smaller size of the experiment compared to the Snowflake microreactor and second, the use of high-enriched uranium fuel in the experiments versus the use of only high-assay low-enriched uranium fuel in the Snowflake microreactor concept. In order to study the effect of these factors, it is useful to plot the normalized flux on a 2D mesh of an XY cross section of the experiment, as shown in Figures 5.2 to 5.4 below. Also included in Figure 5.5 is the energy deposition on an XY mesh.

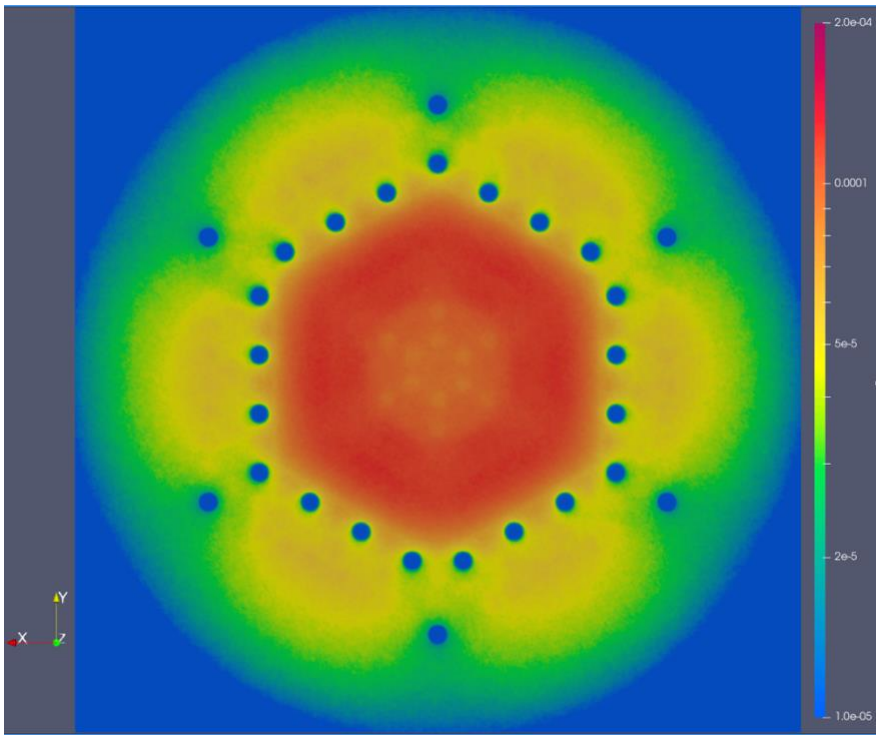

Figure 5.2. Thermal neutron (E < 0.625 eV) normalized flux of experiment v2 [32]

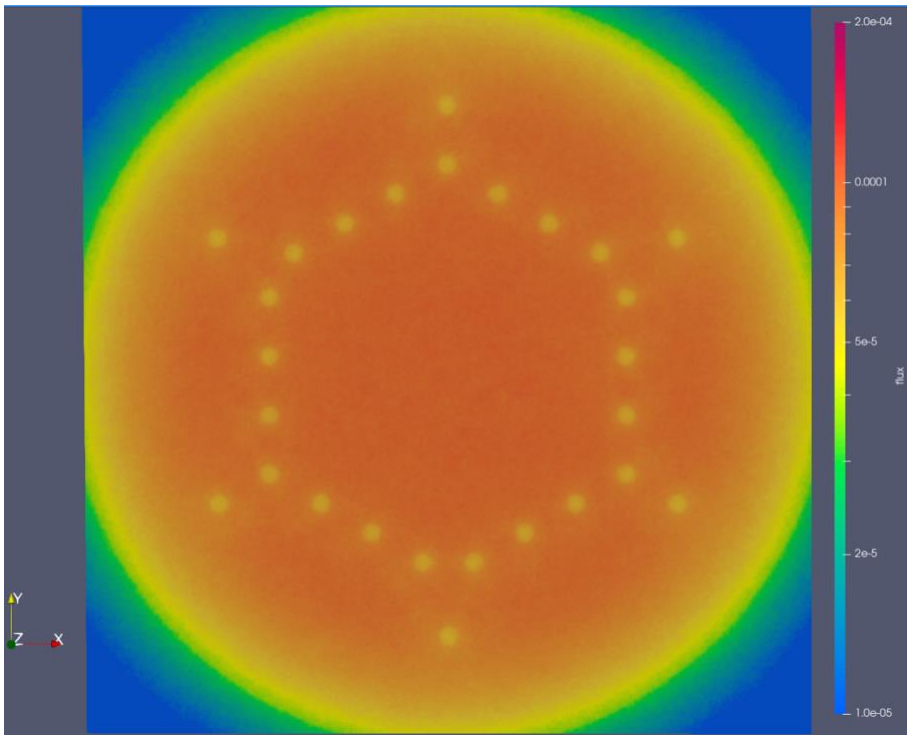

Figure 5.3 Epithermal neutron (0.625 eV < E < 100 keV) normalized flux of experiment v2

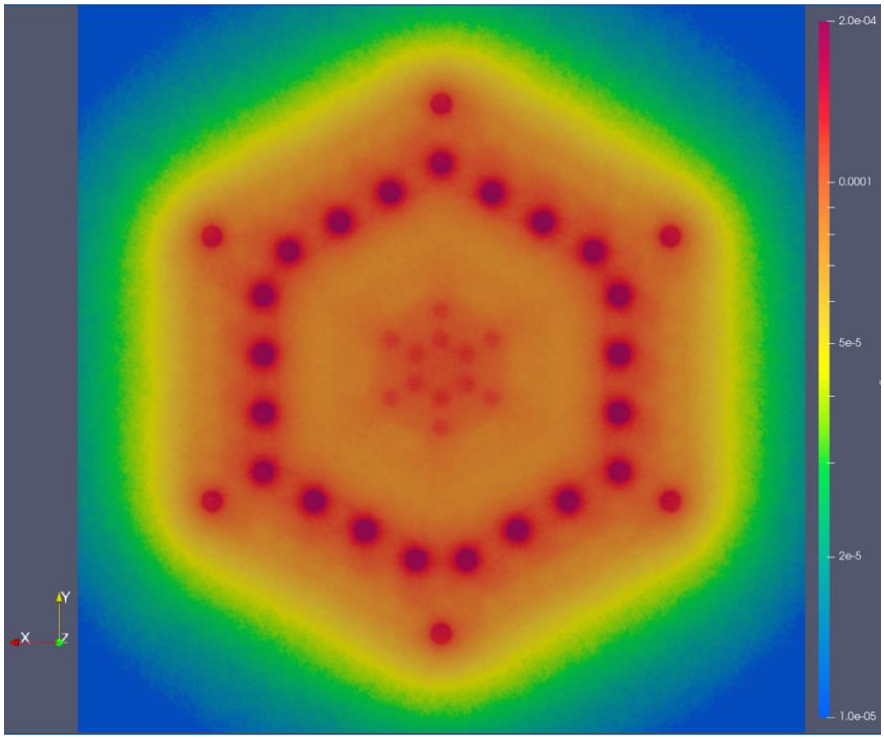

Figure 5.4. Fast neutron (E > 100 keV) normalized flux of experiment v2

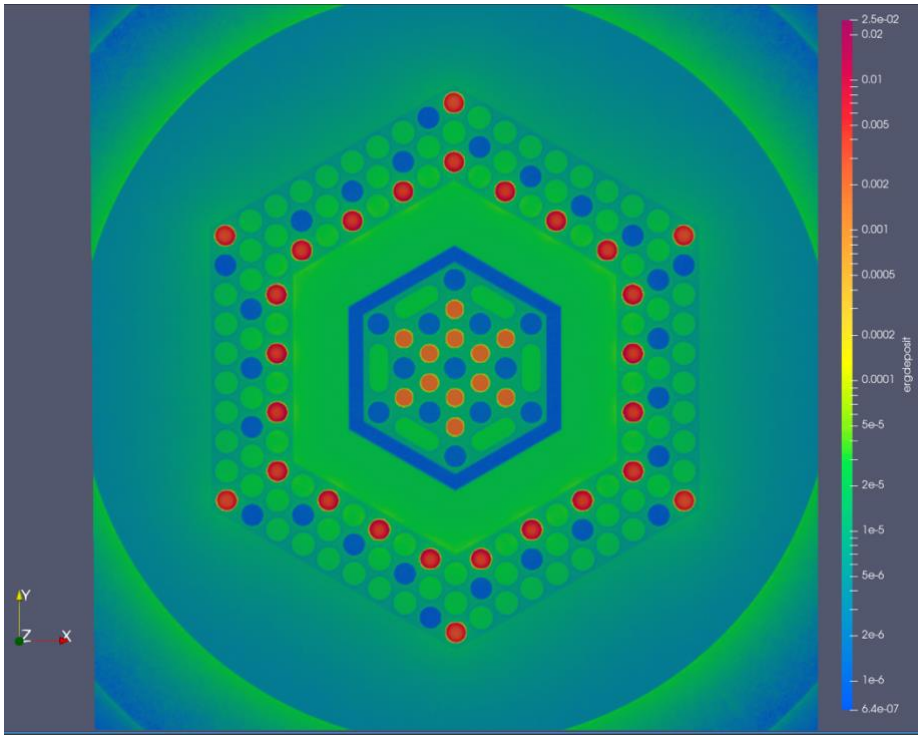

Figure 5.5. Fast neutron (E > 100 keV) normalized flux of experiment v2

The first factor, the size of the experiments versus the full-scale Snowflake microreactor, plays a significant role in the systems. A smaller system is much more likely to leak neutrons due to the volume to surface area ratio compared to a larger system. This means that fission neutrons, which are more likely to be born fast per the Watt distribution, have less distance to scatter and thermalize before either undergoing fission or leaking out of the system in the smaller experiments. As a result, the microreactor experiments all have a higher percentage of fast neutrons causing fission and a lower percentage of thermal neutrons causing fission compared to the Snowflake microreactor. This effect can be noticed visually; the thermal neutron flux (Figure 5.2) is large and round because the neutrons are thermalizing in the outer periphery. The higher leakage fraction of the experiments relative to the full-scale microreactor would explain why the experiments with higher correlation coefficients tend to have a higher mass of metal hydrides;

the hydrides are able to efficiently thermalize neutrons in the small space, better matching the full-scale Snowflake microreactor percentage of thermal neutrons causing fission.

The second factor, the use of high-enriched uranium fuel in the microreactor experiments versus the use of only high-assay low-enriched uranium fuel in the Snowflake microreactor concept is also visually represented in Figures 5.2 and 5.4. Fairly prominently, it can be seen that the highly-enriched fuel in the outer region in thermal neutron flux plot (Figure 5.2) is not seeing much of the thermal flux. This is due to the high absorption of thermal neutrons, causing a depression in the thermal neutron flux. The opposite is true for the fast neutron flux (Figure 5.4); the largest share of fast neutrons originates from the highly-enriched fuel due to the large number of fissions in the fuel. The fast neutron flux looks the most similar to the energy deposition plot (Figure 5.5) which makes sense; the origin of fast fission neutrons will deposit large amounts of energy meaning the fuel will have the largest percentage of energy deposition in the system from primary neutron particles.

The normalized neutron flux per unit lethargy for the inner and outer regions of the experiments is also studied in Figures 5.6 and 5.7 respectively. By taking a look at the different experiment spatial regions, Figures 5.6 and 5.7 are adding additional neutron energy detail to Figures 5.2 to 5.4 which plot the spatial neutron flux on the XY plane. As anticipated, the outer region contains a larger fraction of fast neutrons, due to the large amount of fission neutrons produced by the highly-enriched uranium fuel. The opposite is true for the inner region, which contains a larger fraction of thermal neutrons likely due to the large quantities of moderator between the outer and inner region. Figure 5.1, which plots the normalized neutron flux per unit lethargy for the whole experiment system, is the spatial-weighted average of Figures 5.6 and 5.7.

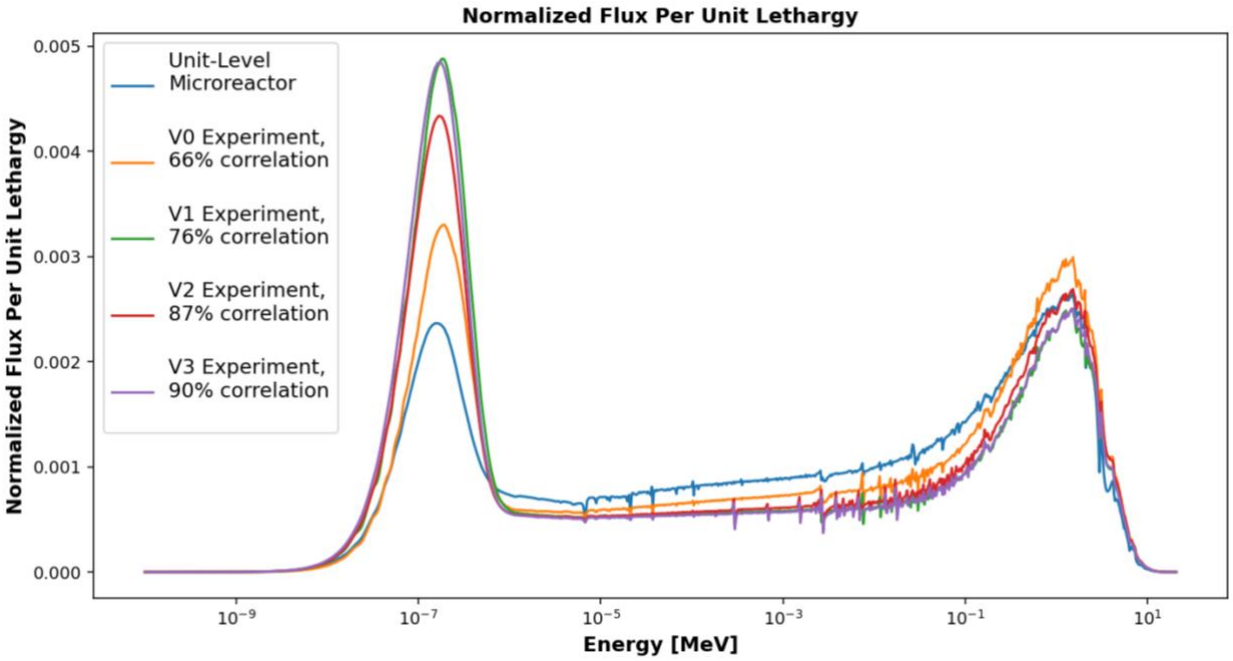

Figure 5.6. Normalized flux per unit lethargy with respect to neutron energy for inner region

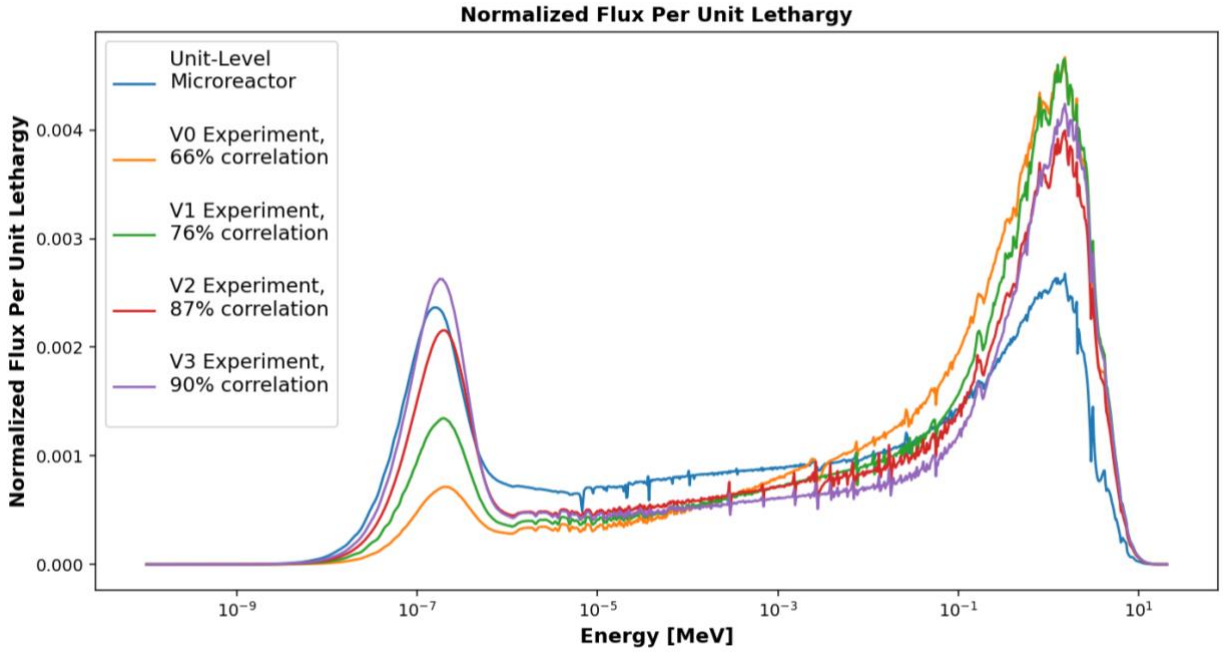

Figure 5.7. Normalized flux per unit lethargy with respect to neutron energy for outer region

The analysis for Figures 5.6 and 5.7 shows how two regions can have competing factors that affect the entire system's reactivity and correlation coefficient. In a small experiment, there is strong interplay with all regions of an experiment; the different impacts of the effective multiplication factor can be captured with a correlation and sensitivity coefficient analysis.

When analyzing the normalized flux per unit lethargy, it is important to understand the difficulty in balancing the many competing factors. For example, a thermal flux will have a different effect on the system's reactivity if there is significantly more uranium-238 present instead of uranium-235. In the same way, the full-scale microreactor (more uranium-238 than uranium-235) will react differently to the same neutron flux than the experiments (more uranium-235 than uranium-238). This concept also applies to the size of the system; a neutron flux will have a different effect on a large system (microreactor) versus a smaller system (experiments) which tends to leak a larger fraction of neutrons.

The neutron flux in a system represents all neutrons that exist *including* the fraction of neutrons that leak, scatter, fission, etc. If the neutrons in this flux leak, they will have less of an impact on the system's effective multiplication factor. Hence sensitivity coefficients, which quantify the impact on the system's effective multiplication factor for all nuclear data parameters at all neutron energies, are better suited to assess neutronic similarity. Alternatively, a better "rule-of-thumb" to assess neutronic similarity that would be better than the flux, but not as robust as correlation/sensitivity coefficients, would be looking at the percentage of neutrons causing fission as shown in Table I. By looking at the percentage of neutrons causing fission, you are limiting yourself to only fission interactions, but these play a significant role in the effective multiplication factor of the system and hence serve as a better measure of neutronic similarity than the neutron flux.

To further explore the feasibility of utilizing the percentage of neutron energies causing fission, the power deposition of the Snowflake microreactor concept and the experiments is plotted with respect to neutron energy in Figure 5.8.

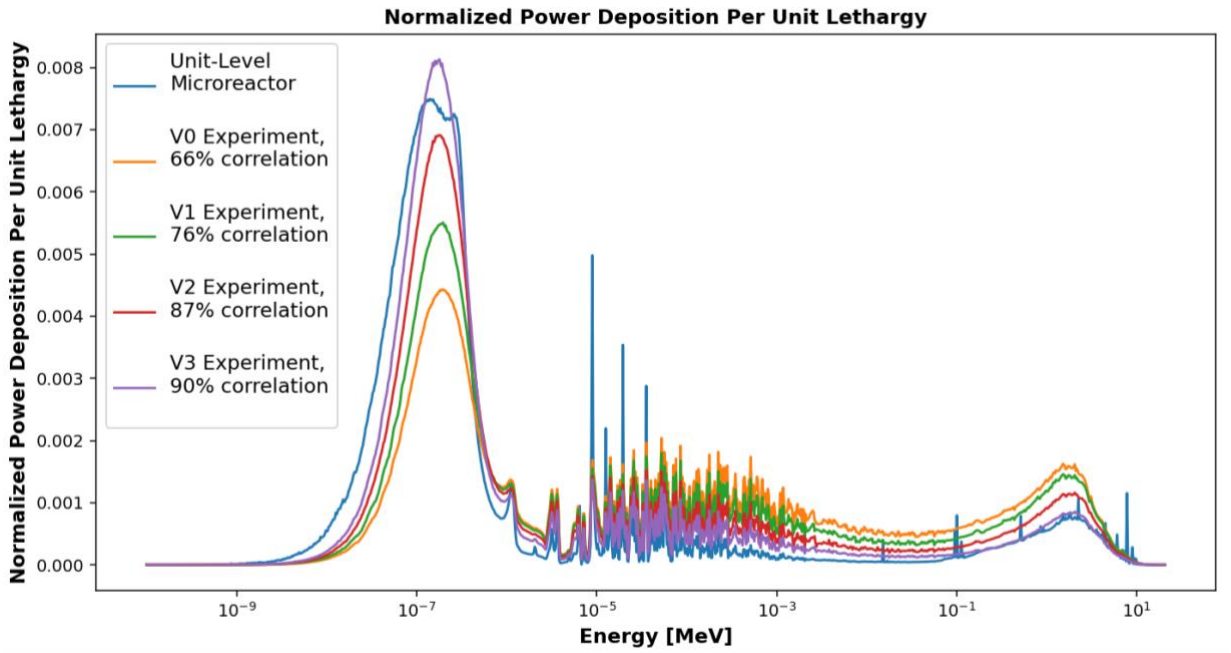

Figure 5.8. Normalized power deposition per unit lethargy with respect to neutron energy

Qualitatively looking at Figure 5.8 shows experiments v2 and v3 are most similar to the full-scale Snowflake microreactor in the thermal region, between 10^{-7} to 10^{-6} [MeV] incident neutron energy. This makes sense since the two experiments have the highest correlation coefficients and power deposition occurs as a result of neutrons undergoing fission, a process that strongly affects the effective multiplication factor. In the fast region (>10^{-1} [MeV] neutron energy), experiment v3 is most similar to the full-scale Snowflake microreactor. Both the fast and the epithermal regions, which combined span 10^{-6} to 10^{1} neutron energies, show the

experiments converging towards the full-scale microreactor power deposition data with increasing correlation coefficient.

To further investigate this trend, the power deposition of the inner and outer regions of the experiments are plotted in Figures 5.9 and 5.10.

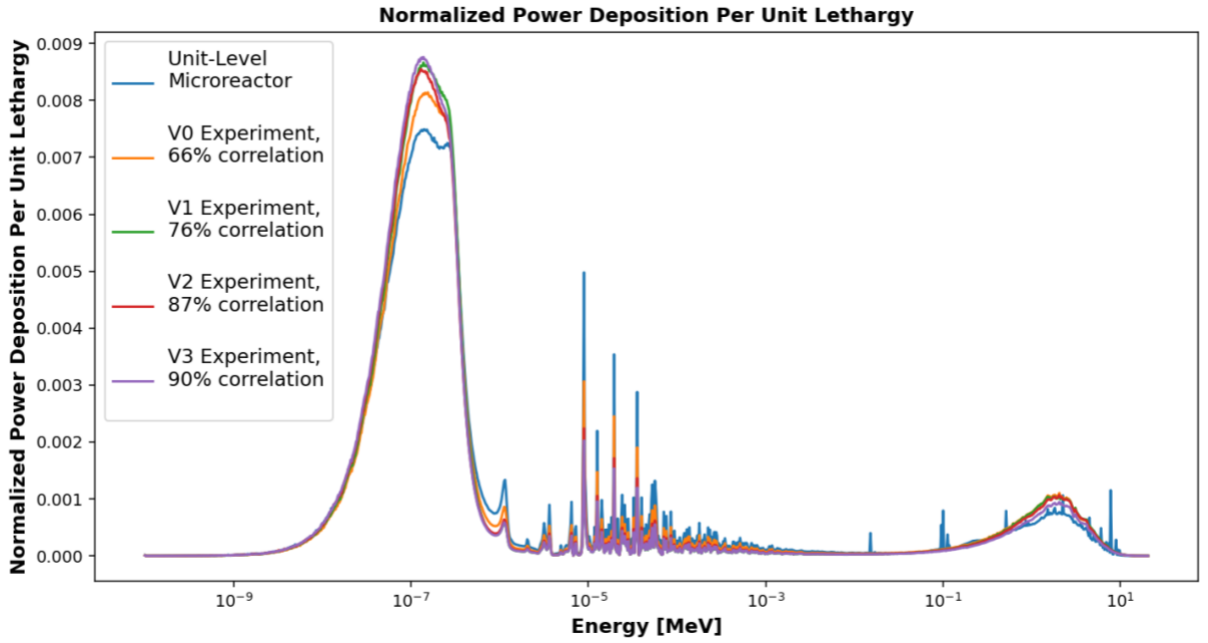

Figure 5.9. Power deposition with respect to neutron energy for experiment inner region

As anticipated from past plots, the inner region of the experiments tends to see a higher fraction of power deposition at thermal neutron energies. Qualitatively inspecting the thermal and epithermal energy regions of Figure 5.9 show experiment v0 data is more similar to the full-scale Snowflake microreactor concept. At high neutron energies, experiment v3 is most similar to the power deposition distribution of the full-scale microreactor concept.

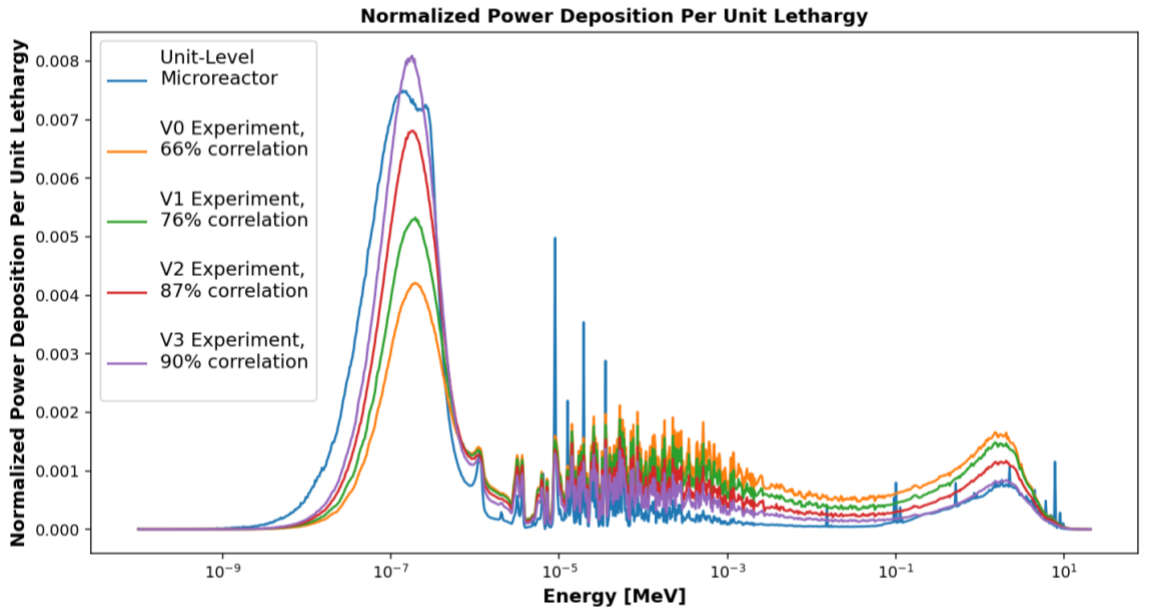

Figure 5.10. Power deposition with respect to neutron energy for experiment outer region

The outer region shown in Figure 5.10 is quite similar to Figure 5.8 upon qualitative inspection; this implies the outer region dominates the power deposition distribution of the whole experiment. This is most likely due to the large amounts of fissions occurring as a result of the high-enriched uranium fuel in the outer region. The same trends appear here; experiment v3 is most similar to the full-scale microreactor concept at all neutron energies. Figure 5.10 represents the challenge of utilizing high-enriched uranium; the experiment requires sufficient reactivity in a small space, but the inner region is what contains the microreactor concept unit cell.

Would this experiment, which the outer region dominates with regards to a higher fraction of power deposition, still be useful to conduct? The answer is yes and this experiment can be justified via correlation coefficients. Even though the outer region provides the majority of fissions and fission neutrons, a 90% correlation coefficient means 90% of the nuclear data uncertainty with regards to effective multiplication factor, is shared between experiment v3 and microreactor concept. Therefore, any discrepancies between the model/simulation and the

experiment that arise due to nuclear data uncertainties will inform the reactor analysts. This benefits the microreactor model as well since analysts will know to anticipate these uncertainties and their effects on the effective multiplication factor. Furthermore, reactivity worth of the inner region and individual components of the microreactor can still be measured and validated.

Power deposition is an important metric to consider and these results show it is a better indicator of neutronic similarity than the flux for these particular configurations. However, to be able to quantify the competing effects of all nuclei-neutron interactions at all energy levels, at all material temperatures, and at all spatial configurations by qualitatively looking at a plot is too challenging. Correlation coefficients, which handle these numerous parameters with sensitivity coefficients, are able to robustly take into consideration all of these competing factors in order to provide an objective metric of neutronic similarity.

Section 5.2. Sensitivity coefficient analyses

To gain further insight into the results, a sensitivity coefficient comparison is conducted for the microreactor experiments and the full-scale Snowflake microreactor concept as shown in Figures 5.9 to 5.12, plotted with Python's Matplotlib [25]. By looking at the specific sensitivity coefficients, we can ensure that there is sufficient coverage for specific nuclides, i.e., the experiment is sensitive to nuclides of interest in the same manner as the full-scale system. Nuclides of interest tend to be the nuclides that are present in large quantities, have the most nuclear data uncertainty, and have the least amount of experimental data/experience in nuclear systems. By designing an experiment that is sensitive to these nuclides of interest in the same manner as the full-scale Snowflake microreactor concept, any discrepancies in the model versus the experiment will inform the analysts and designers of gaps in either the simulations or the nuclear data. This effectively reduces programmatic risk at a fraction of the cost of building a full-scale prototype reactor.

For these experiments, the chosen nuclides and reactions of interest are the uranium-235 fission, carbon-12 elastic scatter, beryllium-9 (n, 2n), and hydrogen-1 elastic scatter sensitivity coefficients.

The uranium-235 sensitivity coefficients (Figure 5.9) provide a clear example of how the experiments, with increasing correlation coefficients, converge towards the sensitivity coefficients of the full-scale Snowflake microreactor system. Since uranium-235 plays a large role in the neutronics of this system, the sensitivity to its fission cross section will have a significant impact on the correlation coefficient by definition. The magnitude of the sensitivity coefficient is significant; the higher the sensitivity coefficient, the more sensitive the system is to

the nuclide cross section at that neutron energy. As expected, uranium-235 has the highest sensitivity coefficient peak at thermal neutron energy levels [35].

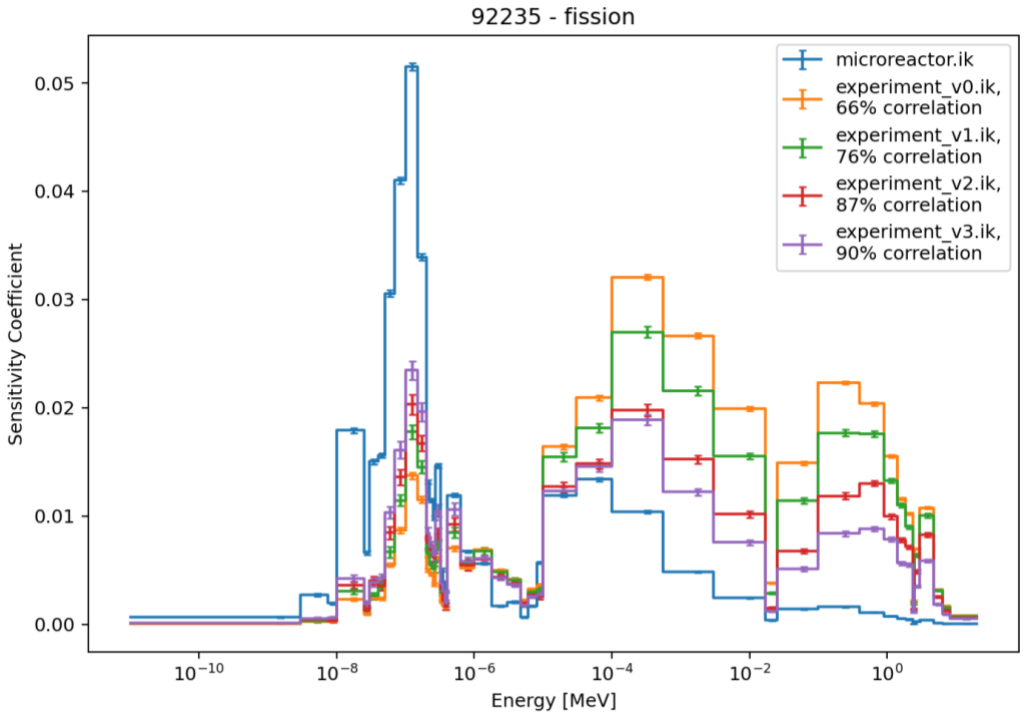

Figure 5.9. Uranium-235 fission sensitivity coefficients

It is interesting to note how the thermal region of the uranium-235 fission sensitivity coefficients are converging to the full-scale microreactor system from a lower sensitivity. In the fast region, the opposite is true; the sensitivity coefficients are converging to the full-scale microreactor system from a higher sensitivity. This is due to the larger role fast fission play in the experiments compared to the full-scale microreactor system; increase importance in the fast neutron region will mean the system is more sensitive to the fast region of the uranium-235 fission cross section.

This behavior, where the fast neutrons add sensitivity to the nuclear data, can also be seen in the hydrogen-1 elastic scattering sensitivities (Figure 5.10). The fast region of the experiments is higher than then thermal region. The opposite is true for the full-scale Snowflake microreactor hydrogen-1 sensitivities; the full-scale microreactor is more sensitive at thermal neutron energy levels.

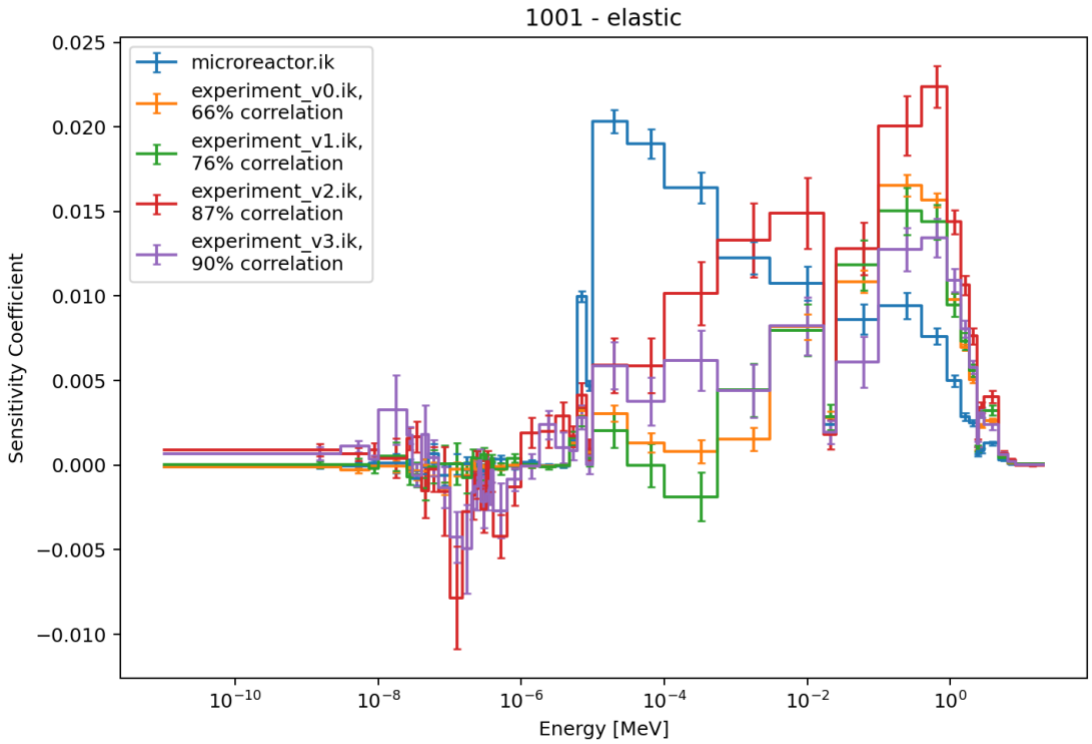

Figure 5.10. Hydrogen-1 elastic scatter sensitivity coefficients

The graphite elastic scattering sensitivities as show in Figure 5.11 are interesting; the experiment with the lowest correlation coefficient appears to have the most similar sensitivity coefficient here, particularly at the higher neutron energies. An error analysis shown in Figure H supports this finding. The reason for the similar sensitivity to graphite lies in the fact that

experiment v0 has the most graphite of the experiments. The higher importance of the uranium-235 fission sensitivity masks the effects of the graphite sensitivity on the correlation coefficient. This competing effect is also shown in Figure 5.13. If an analyst is more interested in studying graphite, it may be more beneficial to select experiment v0 since the sensitivity matches more closely. This case highlights the importance of conducting a sensitivity coefficient analysis for materials of interest.

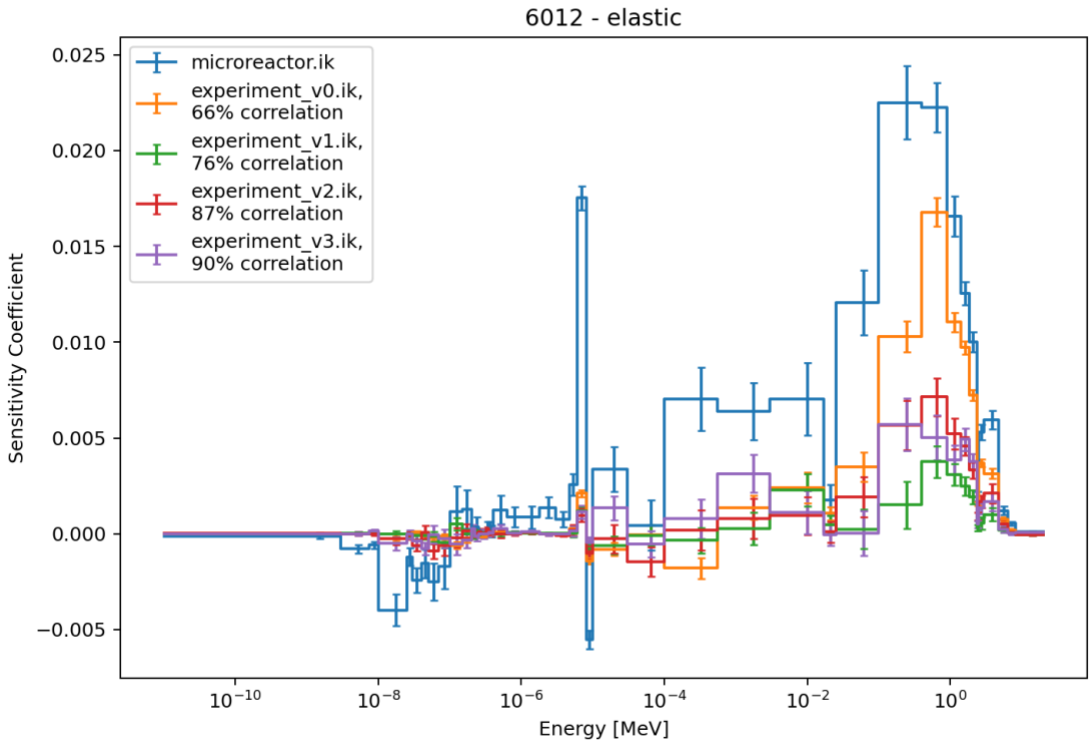

Figure 5.11. Carbon-12 elastic scatter sensitivity coefficients

The final sensitivity studied is the beryllium-9 (n,2n) sensitivity as shown in Figure 5.12. As shown in the beryllium-9 cross section plot back in Chapter 2, Section 5, the (n,2n) reaction only appears at fast neutron energies. This explains why the sensitivity coefficient is zero at

thermal and epithermal neutron energies; they have no effect on the multiplication factor of the system. This sensitivity coefficient highlights how reliant the experiments are on the beryllium reflector. Compared to the full-scale Snowflake microreactor, the experiments are nearly five times more sensitive to the beryllium (n,2n) sensitivity. The experiments, due to their smaller size, are much more affected by neutron leakage than the full-scale Snowflake microreactor.

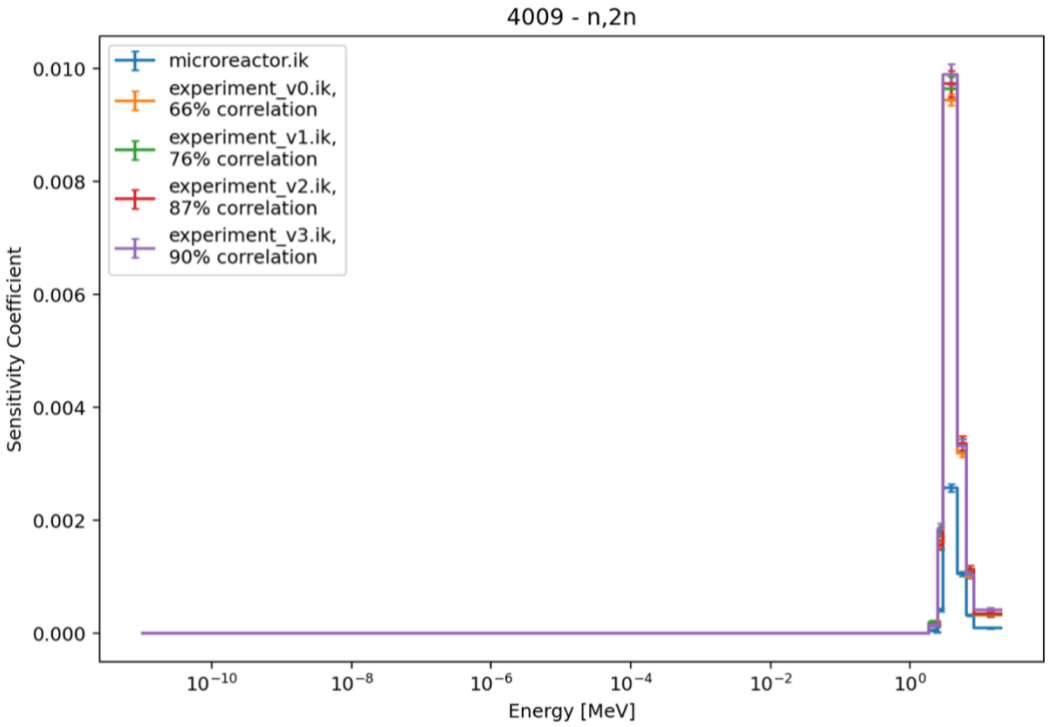

Figure 5.12. Be-9 (n, 2n) sensitivity coefficients

When analyzing the sensitivity coefficients for beryllium, carbon, and hydrogen, it is difficult to determine which sensitivities are most similar to the full-scale microreactor. One way to compare these sensitivities would be with an L2 error analysis as seen in Figure 5.13 and described by $|\mathbf{s}| = \sqrt{\sum_{i=0}^{E} \left|s_{0,i} - s_{1,i}\right|^2}$ where $|\mathbf{s}|$ is the L2 error of the sensitivity coefficient,

$\sum_{i=0}^{E}$ is the summation over all energies, $s_{0,i}$ are the sensitivity coefficients of the full-scale Snowflake microreactor, and $s_{1,i}$ are the sensitivity coefficients of the microreactor experiments. An L2 error analysis measures the least squares error; conceptually, this analysis measures the spread of the data. The closer the microreactor experiments' sensitivity coefficients are to the full-scale Snowflake microreactor sensitivity coefficients at each neutron energy, the lower the L2 error. It is important to note that this L2 error analysis does not weigh the error with respect to neutron energy which may need to be done for a more robust analysis.

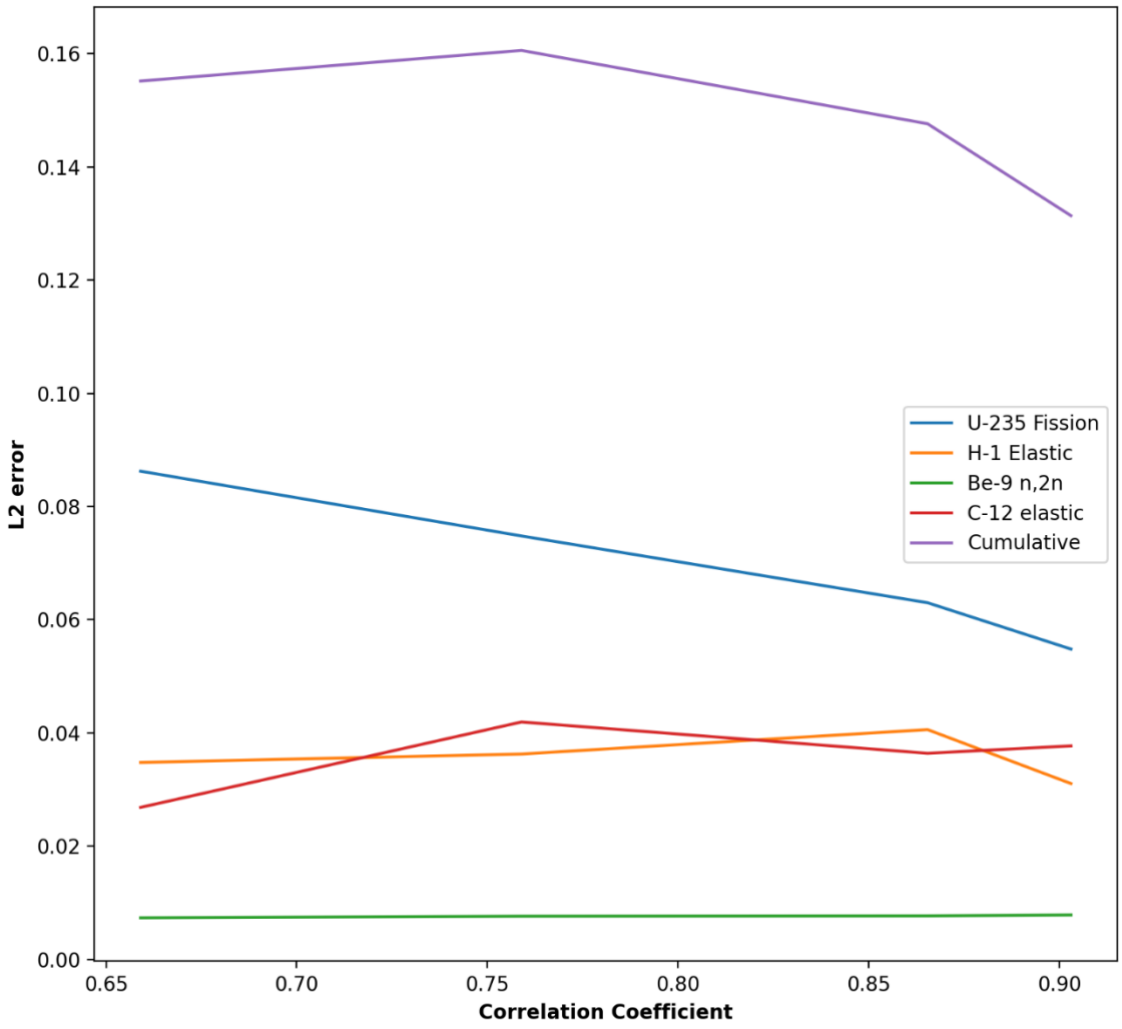

Figure 5.13. L2 error of sensitivity coefficients with respect to correlation coefficient

The most dominant sensitivity, after being weighed with the nuclear data covariance matrix, will be prioritized when folding all of the data into the correlation coefficient. This is evident when studying Figure 5.13; the uranium-235 fission sensitivity coefficient error most closely follows the cumulative L2 error, both of which decrease steadily with increasing correlation coefficient. This analysis highlights why it is important to conduct a sensitivity coefficient study. If a specific cross section or material is of higher interest than the uranium-235 fission sensitivity for this particular configuration, then it should be prioritized. However, for this scope, the overall system is of interest and a single cross section or material is not prioritized in this analysis.

The patterns and behaviors shown in this research may oftentimes not be intuitive, which highlights the importance of conducting a sensitivity and correlation coefficient analysis. These analyses provide further evidence of neutronic similarity between two systems and serve to increase the robustness with regards to how we design nuclear experiments for advanced reactor concepts.

Chapter 6 – Conclusion

The goal of this research is to study correlation coefficients as an objective way to design the neutronic aspects of microreactor experiments which will aide in microreactor design, validation, and the eventual construction of a full-scale microreactor system. Nuclear experiments are needed to validate existing physics codes and serve as an intermediate to a full-scale prototype microreactor. The mathematics and physics of this research are also general enough to be applied to other advanced reactor concepts; microreactors were simply the focus for this particular research.

Both the use of high-enriched uranium fuel and the size differences for this particular experiment and full-scale microreactor design pose a burden; how do we know if the two systems are neutronically similar? Correlation coefficients are one objective way to assess the neutronic similarity between two systems and should be included in conjunction with other neutronic analyses. This research shows that smaller-scale nuclear experiments can be useful in validating simulations of a full-scale microreactor system because we can tailor the neutronics to be representative of the system of interest via correlation coefficients. Additionally, this analysis gauges how sensitive the experiments and full-scale microreactor concepts are with regards to reactivity and all available neutron-nuclei interactions.

Furthermore, this research demonstrates that the percentage of fissions caused by thermal neutrons can be used to roughly guide new designs to a higher correlation coefficient as long as similar materials are being used since the fission sensitivity plays a large role in nuclear systems. When looking at the sensitivity coefficients, this study demonstrates the neutronic importance of uranium-235 for these two systems in particular. It is important to conduct a sensitivity and correlation coefficient analysis to reveal additional, sometimes non-intuitive, information about

the systems being analyzed. A sensitivity and correlation coefficient analysis comprehensively includes a plethora of neutron-nuclei interactions and their related uncertainties, making this method a robust way to compare the neutronics of two systems.

Limitations to this work include the fact that correlation and sensitivity coefficient analyses at the moment are steady-state. Conducting these analyses at different temperatures, different depletion levels, and different reactor configurations, such as varied control drum positions for microreactors, will provide a more robust analysis. Additionally, correlation and sensitivity coefficient analyses consider only the neutronics with regards to the impact of effective multiplication factor. Reaction rate sensitivities, for example, look at how particular reaction rates in a system react to perturbations; this type of analysis would be useful to conduct if an analyst is interested in a particular material or region of the experiment (such as the inner region) and wishes to further characterize and quantify uncertainties related to the material [37]. A reaction rate sensitivity analysis would also be useful to study the inner regions of these various experiments. Matching reaction rate sensitivities of the inner region of the experiment with a unit cell at a particular spatial point in the conceptual microreactor would serve as a beneficial additional experiment to conduct in order to accurately measure reactivity worth of various reactor components. Furthermore, reactor designs may have equally important physics, such as thermal hydraulics or thermal mechanics physics, that need to be characterized and considered in conjunction with a correlation and sensitivity coefficient analysis.

The neutronics framework outlined in this research serves as a starting point for experiment neutronic design; additional work must be conducted with other physics codes (thermal mechanics, heat transfer, etc.) in order to design a successful experiment. Future work includes developing a framework to assess the similarity between the transient behavior of an

experiment and a full-scale microreactor; this will necessitate transient neutronics and heat transfer physics codes, as well as building on existing steady-state similarity/correlation coefficients. Additionally, further consideration to manufacturing, budget, and other realistic limitations should be analyzed and factored into the experiment design early in the overall process.

References

1. International Energy Agency (2019). *Electricity*. Retrieved from https://www.iea.org/fuels-and-technologies/electricity
2. Ritchie, H. (2020). *What are the safest and cleanest sources of energy?* Retrieved from https://ourworldindata.org/safest-sources-of-energy
3. *Nuclear Microreactors*. U.S. Government Accountability Office. Retrieved from https://www.gao.gov/products/gao-20-380sp
4. Armstrong, J., Brown, F., Bull, J., et. al. (2017). "MCNP USER'S MANUAL Code Version 6.2". *Los Alamos National Laboratory.* LA-UR-17-29981.
5. Brown, F. B., Rising, M. E., Alwin, J. L., et. al. (2017). "User Manual for Whisper-1.1." *Los Alamos National Laboratory*. LA-UR-17-20567.
6. Trellue, H. R., Rao, D. V., Wilkerson, R. B., Kim, J., Luther, E. and Fallgren, A. (2020) "Simulation of Microreactor Design With Graphite Core Block, TRISO fuel, Heat Pipes, and Yttrium Hydride Moderator", *U.S. Provisional Patent Application 1620.0121P*, DOE Reference S-133,840.000." Los Alamos National Laboratory. LA-CP-20-20306.
7. *History of USS Nautilus.* Retrieved from https://ussnautilus.org/history-of-uss-nautilus/
8. *Microreactors could replace diesel generators, enable renewables, report says*. Idaho National Laboratory. Retrieved from https://inl.gov/article/microreactors-could-replace-diesel-generators-enable-renewables-report-says/
9. Voss, S. (1984). "SNAP Reactor Overview." *Kirtland AFB, New Mexico: U.S. Air Force Weapons Laboratory.* AFWL-TN-84-14.
10. Erickson, G. (1960). *George Erickson and the birth of the heat pipe*. Retrieved from https://www.lanl.gov/discover/publications/connections/2018/2018-07/science.php

11. McClure, P. R., Poston, D. I., Dixon, D. D. (2012). “Final Results of Demonstration Using Flattop Fissions (DUFF) Experiment.” *Los Alamos National Laboratory*, LA-UR-12-25165.
12. Poston, D. I., Gibson, M. A., Godfroy, T., et. al. (2020). “KRUSTY Reactor Design.” *Nuclear Technology*, volume 206(17), pp. 13–30.
13. *KRUSTY project demonstrates potential power sources for future space exploration.* National Nuclear Security Administration. Retrieved from https://www.energy.gov/nnsa/articles/krusty-project-demonstrates-potential-power-sources-future-space-exploration
14. Shivprasad, A.P., Cutler, T. E., Jewell, J. K. (2020). “Advanced Moderator Material Handbook.” *Los Alamos National Laboratory.* LA-UR-20-27683.
15. Cutler, T, Trellue, H. R., Blood, M., et. al. (2021). “The Hypatia Experiment: Yttrium Hydride - HEU Critical Experiment”. *Los Alamos National Laboratory*. LA-UR-21-22920.
16. Grabaskas D. (2019). “Heat-Pipe Microreactors.” *Argonne National Laboratory*
17. Shivprasad, A. P., Frazer, D. M., Mehta, V. K., Cooper, M. W. D. and Saleh, T.A. (2020) “Elastic moduli of high-density, sintered monoliths of yttrium dihydride.” *Journal of Alloys and Compounds*, volume 826(14), p. 826.
18. Mehta, V. K. Cooper, M. W. D., and Wilkerson, R. B. (2020). “Evaluation of Yttrium Hydride (-YH2-x) Thermal Neutron Scattering Laws and Thermophysical Properties.” *Nuc Sci Eng*. volume 195(14). pp. 563–577.

19. Soppera, N., Bossant, M., Dupont, E. (2014) "JANIS 4: An Improved Version of the NEA Java-based Nuclear Data Information System." *Nuclear Data Sheets*. Volume 120. Pages 294-296.
20. Office of Nuclear Energy. *TRISO Particles: The Most Robust Nuclear Fuel on Earth*. Retrieved from https://www.energy.gov/ne/articles/triso-particles-most-robust-nuclear-fuel-earth
21. Read, E. A., Trellue, H. R., and Oliveira, C. R. E. D. (2011). "Assessment of Three-dimensional Monte Carlo Burnup for Gas Cooled Reactors Using the Reactivity Equivalent Physical Transformation Method." *M&C*.
22. Greenwood, N. N., Earnshaw, A. (1997). "Chemistry of the Elements (2nd ed.)." *Butterworth-Heinemann*. ISBN 978-0-08-037941-8.
23. Lamarsh, J. R. (1983). "Introduction to Nuclear Reactor Theory". 2nd ed. *Addison-Wesley*. Reading. MA.
24. Adams, M. L. (2017). "Introduction to Nuclear Reactor Theory." *Texas A&M University*
25. CERN Indico. "The Fission Spectrum"
26. Hunter, J. D. (2007). "Matplotlib: A 2D graphics environment", *Computing in Science & Engineering*, Volume 9, Number 3, Pages 90--95, IEEE COMPUTER SOC, 10.1109/MCSE.2007.55.
27. Perfetti, C. (2020). "The Adjoint Boltzmann Transport Equation (Online Lecture)." Retrieved at https://www.youtube.com/watch?v=uEBOylmfZk4
28. Kiedrowski, B.C., Brown, F., et al. "Adjoint-Based k-Eigenvalue Sensitivity Coefficients to Nuclear Data Using Continuous-Energy Monte Carlo"

29. Kiedrowski, B.C., Brown, F., et al. (2017). “Whisper: Sensitivity/Uncertainty-Based Computational Methods and Software for Determining Baseline Upper Subcritical Limits.” *Nucl Sci Eng*, volume 181(1), pp. 17–47.
30. B. Broadhead, B. Rearden, C. Hopper, and et. al. “Sensitivity-and Uncertainty- Based Criticality Safety Validation.” Nucl Sci Eng, volume 146(3), pp. 340–366 (2004).
31. NEVADA NATIONAL SECURITY SITE. (2011). “National Criticality Experiments Research Center”
32. Microsoft Corporation. (2018). *Microsoft Excel*. Retrieved from https://office.microsoft.com/excel
33. Ahrens, J., Geveci, B., Law, C., (2005) “ParaView: An End-User Tool for Large Data Visualization, Visualization Handbook.” *Elsevier*. ISBN-13: 978-0123875822. ANS Winter Meeting
34. Rossum, V. G., Drake, F. L. (2009). “Python 3 Reference Manual.” Scotts Valley, CA: *CreateSpace*.
35. Maldonado, A, Perfetti, C. M., Trellue, H. R., Blood, M. (2021). “Neutron Spectra and Correlation Coefficient Convergence When Designing a Microreactor Experiment with MCNP/Whisper.” *ANS Transactions*
36. Maldonado, A, Perfetti, C. M., Trellue, H. R. (2022). “MCNP and Whisper Neutronics Framework for Designing Microreactor Experiments.” *PHYSOR*
37. Perfetti, C. M., et. al. (2017). “Sensitivity Coefficients for Diffusion Coefficients and Other Reactor Physics Parameters using CE TSUNAMI-3D.” *USDOE*.